

Fiber orientation distributions based on planar fiber orientation tensors of fourth order

Mathematics and Mechanics of Solids
1–22

© The Author(s) 2022



Article reuse guidelines:

sagepub.com/journals-permissions

DOI: 10.1177/10812865221093958

journals.sagepub.com/home/mms**Julian Karl Bauer** *Institute of Mechanics, Karlsruhe Institute of Technology (KIT), Karlsruhe, Germany***Thomas Böhlke** *Chair for Continuum Mechanics, Institute of Engineering Mechanics, Karlsruhe Institute of Technology (KIT), Karlsruhe, Germany*

Received 19 November 2021; accepted 24 March 2022

Abstract

Fiber orientation tensors represent averaged measures of fiber orientations inside a microstructure. Although, orientation-dependent material models are commonly used to describe the mechanical properties of representative microstructure, the influence of changing or differing microstructure on the material response is rarely investigated systematically for directional measures which are more precise than second-order fiber orientation tensors. For the special case of planar orientation distributions, a set of admissible fiber orientation tensors of fourth-order is known. Fiber orientation distributions reconstructed from given orientation tensors are of interest both for numerical averaging schemes in material models and visualization of the directional information itself. Focusing on the special case of planar orientations, this paper draws the geometric picture of fiber orientation distribution functions reconstructed from fourth-order fiber orientation tensors. The developed methodology can be adopted to study the dependence of material models on planar fourth-order fiber orientation tensors. Within the set of admissible fiber orientation tensors, a subset of distinct tensors is identified. Advantages and disadvantages of the description of planar orientation states in two- or three-dimensional tensor frameworks are demonstrated. Reconstruction of fiber orientation distributions is performed by truncated Fourier series and additionally by deploying a maximum entropy method. The combination of the set of admissible and distinct fiber orientation tensors and reconstruction methods leads to the variety of reconstructed fiber orientation distributions. This variety is visualized by arrangements of polar plots within the parameter space of fiber orientation tensors. This visualization shows the influence of averaged orientation measures on reconstructed orientation distributions and can be used to study any simulation method or quantity which is defined as a function of planar fourth-order fiber orientation tensors.

Keywords

Fiber orientation tensor, anisotropy, fiber-reinforced composites, maximum entropy method

Corresponding author:

Julian Karl Bauer, Institute of Mechanics, Karlsruhe Institute of Technology (KIT), Otto-Ammann-Platz 9, 76131 Karlsruhe, Germany.

Email: julian.bauer@kit.edu

1. Introduction

Suitable microstructure descriptors are essential for the prediction of effective properties of fiber-reinforced composites. Fiber orientation distribution functions (FODFs) represent exact microstructure descriptors of the orientation of axisymmetric fibers within a specified volume of a fiber-reinforced composite [1,2]. However, in practice [3,4], the exact distribution of fibers is commonly approximated by fiber orientation tensors which represent averaged directional measures and can be directly determined by non-destructive analysis methods, such as computer tomography [5,6]. Furthermore, fiber orientation tensors fit into the tensor-based framework of continuum mechanics which is frequently used in material modeling [7–9]. The dependence of material models on the set of admissible second-order fiber orientation tensors is studied numerically in, e.g., [10,11]. However, the dependence of material models or other quantities of interest such as reconstructed FODF itself on fourth-order fiber orientation tensors is rarely studied analytically. In addition, for some applications, e.g., damage modeling [12] or averaging schemes [8,9], the identification of an FODF based on given fiber orientation tensors is beneficial. Due to the averaged character of fiber orientation tensors, no one-to-one correspondence to an FODF exists. Nevertheless, for a given fiber orientation tensor, any associated FODF is of interest and eases the indirect visualization of fiber orientation tensors. Many fiber-reinforced composites are plate-like, and if the mean fiber length is larger than the plate thickness, the resulting fiber distribution is approximately planar. This holds, e.g., for sheet molding compound [4]. For such planar fiber distributions, Bauer and Böhlke [13] identify a set of all admissible fourth-order fiber orientation tensors. Based on this set and reconstruction methods following [1,14], the variety of reconstructed FODF based on planar fiber orientation tensors of fourth-order is studied in the current work.

This paper is structured as follows. Definitions of FODF and fiber orientation tensors are followed by a reformulation of planar fiber orientation tensors following Bauer and Böhlke [13]. Within the admissible set of planar fourth-order fiber orientation tensors given by Bauer and Böhlke [13], a subset of distinct planar fourth-order fiber orientation tensors is identified. FODF approximations by truncated Fourier series with planar leading fiber orientation tensors in a three-dimensional (3D) framework are identified as non-planar and motivate a two-dimensional (2D) framework. The reconstruction of FODF based on the maximum entropy method following Müller and Böhlke [14] is recast into this 2D framework. Discrete slices and points of the set of admissible and distinct planar fourth-order fiber orientation tensors are used to visualize reconstructed FODF based on fourth-order fiber orientation tensors. A note on FODF reconstruction solely based on second-order fiber orientation tensors including the exact closure [15] closes this paper.

1.1. Notation

Symbolic tensor notation is preferred in this paper. Tensors of first order are denoted by bold lowercase letters such as \mathbf{q} , \mathbf{n} , \mathbf{v} , \mathbf{e} . Tensors of second order are denoted by bold uppercase letters like \mathbf{N} or \mathbf{Q} and fourth order tensors are denoted by, e.g., \mathbb{N} or \mathbb{D} . Tensors in representations for varying tensor order are represented by, e.g., $\mathbb{D}_{<k>}$, where k defines the tensor order. Tensorial quantities are defined in a 3D space, unless underlined. If a tensor is underlined like, e.g., $\underline{\mathbf{q}}$ or $\underline{\mathbb{N}}$, it is defined in a 2D space and follows this spaces algebra. A linear mapping of a second-order by a fourth-order tensor reads as $\mathbf{A} = \mathbb{C}[\mathbf{B}]$. The scalar product reads as $\mathbf{A} \cdot \mathbf{B}$. The tensor power, i.e., the k th dyadic product of, e.g., a first-order tensor \mathbf{a} is denoted by $\mathbf{a}^{\otimes k}$ yielding, e.g., $\mathbf{a}^{\otimes 3} = \mathbf{a} \otimes \mathbf{a} \otimes \mathbf{a}$. An orthonormal basis is denoted by $\{\mathbf{e}_i\}$ with $\mathbf{e}_i \cdot \mathbf{e}_j = \delta_{ij}$ and the Kronecker delta δ_{ij} . If a matrix of tensor coefficients is used in mixed notation, the coefficient matrix is directly followed by the tensor basis where the first index of the basis corresponds to the rows of the coefficients matrix, and the second one to the columns. Summation convention applies, unless otherwise stated. Representations in index notation always refer to an orthonormal basis. The Rayleigh product is used to represent an active rotation of a physical quantity and for a first-order tensor is defined by $\mathbf{Q} \star \mathbf{n} = n_i \mathbf{Q} \mathbf{e}_i$. Sets, i.e., collections of quantities, are denoted by calligraphic symbols, e.g., \mathcal{F} and are constructed by curly braces. Inside the curly braces, elements of the set are given explicitly, or by a generator expression following the pattern {quantity | condition fulfilled by element contained in set}. Although, this work and related code is based on [16,17], numbering and indices follow the continuum mechanics convention starting at one.

2. Fiber orientation distributions based on planar fiber orientation tensors of fourth order

2.1. Directional measures as microstructure descriptors

Taking the average of a tensorial quantity over orientations requires a directional measure which quantifies the orientations. Established directional measures of axisymmetric fibers are the FODF and fiber orientation tensors of several kinds and orders. Both FODF and fiber orientation tensors quantify orientations inside a reference volume which might be interpreted as a section of specified size at a specific position \mathbf{x} inside a structural component. Consequently, the directional measurement depends on the size of this reference volume which usually represents a scaling parameter in measurement algorithms (see, e.g., Görthofer et al. [4, Figure 4] or Schöttl et al. [6]). This section introduces basic quantities and in large parts follows [13, sections 2.1 and 2.2].

2.1.1. Fiber orientation distribution function. The FODF ψ at a given position inside a component

$$\psi : \mathcal{S}^2 \rightarrow \mathbb{R}, \quad \text{with } \mathcal{S}^2 = \{\mathbf{n} \in \mathbb{R}^3 \mid \|\mathbf{n}\| = 1\}, \quad (1)$$

maps any direction \mathbf{n} onto a scalar value $\psi(\mathbf{n})$. \mathcal{S}^2 is the 2D surface of a unit sphere in three dimensions parameterized by, e.g., a unit vector \mathbf{n} . The function $\psi(\mathbf{n})$ is non-negative, i.e.,

$$\psi(\mathbf{n}) \geq 0, \quad \forall \mathbf{n} \in \mathcal{S}^2, \quad (2)$$

holds and normalization of $\psi(\mathbf{n})$ implies

$$\int_{\mathcal{S}^2} \psi(\mathbf{n}) \, dn = 1. \quad (3)$$

As fibers have a direction but no attitude, $\psi(\mathbf{n})$ is symmetric, i.e.,

$$\psi(-\mathbf{n}) = \psi(\mathbf{n}), \quad \forall \mathbf{n} \in \mathcal{S}^2, \quad (4)$$

holds (see [2,11]).

2.1.2. Fiber orientation tensors. Fiber orientation tensors of Kanatani [1] first kind are defined by

$$\mathbb{N}_{\langle k \rangle} = \int_{\mathcal{S}^2} \psi(\mathbf{n}) \mathbf{n}^{\otimes k} \, dn, \quad (5)$$

with $\mathbf{n}^{\otimes k}$ being the k th moment of \mathbf{n} . In this work, only the second- and fourth-order fiber orientation tensors

$$\mathbf{N} = \mathbb{N}_{\langle 2 \rangle} = \int_{\mathcal{S}^2} \psi(\mathbf{n}) \mathbf{n} \otimes \mathbf{n} \, dn, \quad (6)$$

$$\mathbb{N} = \mathbb{N}_{\langle 4 \rangle} = \int_{\mathcal{S}^2} \psi(\mathbf{n}) \mathbf{n} \otimes \mathbf{n} \otimes \mathbf{n} \otimes \mathbf{n} \, dn, \quad (7)$$

are used. More details on the properties of $\mathbb{N}_{\langle k \rangle}$ can be found, e.g., in Bauer and Böhlke [13]. Higher-order fiber orientation tensors of Kanatani first kind contain all tensors of lower order as

$$\mathbb{N}_{\langle k-2 \rangle} = \mathbb{N}_{\langle k \rangle} [\mathbf{I}], \quad (8)$$

holds for $2 \leq k$ with the identity on second-order tensors $\mathbf{I} = \delta_{ij} \mathbf{e}_i \otimes \mathbf{e}_j$. In addition, for the second-order orientation tensor

$$\mathbf{N} \cdot \mathbf{I} = \text{tr}(\mathbf{N}) = 1, \quad (9)$$

holds due to normalization (see [13]). Orientation tensors of Kanatani first kind are commonly used to represent directional data obtained by computer tomography scans or results of flow simulations [4]. Basic properties of the second-order orientation tensor \mathbf{N} are briefly summarized following Bauer and Böhlke [13]. \mathbf{N} is symmetric and positive semi-definite. In consequence, \mathbf{N} can be diagonalized, i.e., pairs of eigenvalues λ_i with $\lambda_i \geq 0$ and orthonormal eigenvectors \mathbf{v}_i for $i \in [1, 2, 3]$ exist, such that

$$\mathbf{N} = N_{ij}^{(2)} \mathbf{e}_i \otimes \mathbf{e}_j = \sum_{i=1}^3 \lambda_i \mathbf{v}_i \otimes \mathbf{v}_i = \begin{bmatrix} \lambda_1 & 0 & 0 \\ & \lambda_2 & 0 \\ \text{sym} & & \lambda_3 \end{bmatrix} \mathbf{v}_i \otimes \mathbf{v}_j, \quad (10)$$

holds and there exists a rotation defined by an orthogonal tensor

$$\mathbf{Q} = \mathbf{v}_i \otimes \mathbf{e}_i, \quad (11)$$

mapping the arbitrary but fixed basis $\{\mathbf{e}_i\}$ onto the basis $\{\mathbf{v}_i\}$. The orthonormal basis $\{\mathbf{v}_i\}$ spanned by the eigenvectors is, in the following, called orientation coordinate system. Based on the ordering convention

$$\lambda_3 \leq \lambda_2 \leq \lambda_1, \quad (12)$$

an established classification of structurally differing \mathbf{N} exists (see [10, 18–20]). A visualization corresponding to this classification exists and is called orientation triangle. Any second-order orientation tensor can be represented by a pair (λ_1, λ_2) , which is connected to a point inside the orientation triangle and by a mapping \mathbf{Q} which defines the orientation coordinate system. The FODF can be expressed in terms of fiber orientation tensors as a 3D tensorial Fourier series

$$\psi(\mathbf{n}) = \frac{1}{4\pi} \sum_{k=0}^{\infty} \frac{2k+1}{2^k} \binom{2k}{k} \text{dev}(\mathbb{N}_{\langle k \rangle}) \cdot \mathbf{n}^{\otimes k}, \quad (13)$$

which is called spherical harmonic expansion [1, p. 154]. The operator $\text{dev}(\cdot)$ extracts the deviatoric part and its definition for higher-order tensors in a 3D framework is given in Spencer [21]. Equation (13) implies that in general an infinite number of orientation tensors of increasing order is required to express $\psi(\mathbf{n})$. However, for many practical applications, only second- and fourth-order orientation tensors are available at a specific location inside a component. Recent developments in computer tomography methods for fiber-reinforced composites lead toward the identification of the FODF instead of fiber orientation tensors (see, e.g., [22]).

2.2. Admissible and distinct planar fiber orientation tensors

A parameterization of planar fiber orientation tensors of second-order $\mathbf{N}^{\text{planar}}$ is given by

$$\mathbf{N}^{\text{planar}}(\lambda_1) = \lambda_1 \mathbf{v}_1 \otimes \mathbf{v}_1 + (1 - \lambda_1) \mathbf{v}_2 \otimes \mathbf{v}_2 = \begin{bmatrix} \lambda_1 & 0 & 0 \\ & 1 - \lambda_1 & 0 \\ \text{sym} & & 0 \end{bmatrix} \mathbf{v}_i \otimes \mathbf{v}_j, \quad (14)$$

in the orientation coordinate system $\{\mathbf{v}_i\}$ defined in equation (11) and with $1/2 \leq \lambda_1 \leq 1$. Bauer and Böhlke [13, equation (87)] identify planar fiber orientation tensors of fourth-order $\mathbb{N}^{\text{planar}}(\alpha_1, d_1, d_8)$ which can be reparameterized in λ_1 with $\alpha_1 = 4/3(\lambda_1 - 1/2)$ leading to

$$\mathbb{N}^{\text{planar}}(\lambda_1, d_1, d_8) = \left[\begin{array}{ccc|ccc} \lambda_1 - d_1 - \frac{4}{35} & d_1 + \frac{4}{35} & 0 & 0 & 0 & \sqrt{2}d_8 \\ & (1 - \lambda_1) - d_1 - \frac{4}{35} & 0 & 0 & 0 & -\sqrt{2}d_8 \\ & & 0 & 0 & 0 & 0 \\ \hline & & & \text{completely} & & \text{symmetric} \end{array} \right] \mathbf{B}_\xi^v \otimes \mathbf{B}_\zeta^v, \quad (15)$$

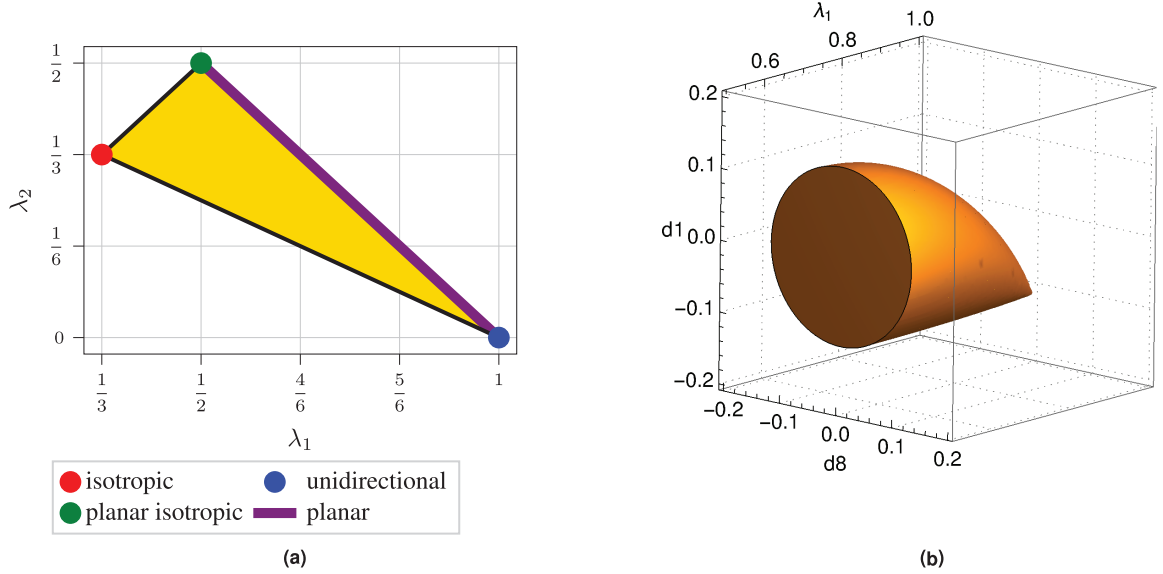


Figure 1. (a) Orientation triangle visualizing second-order orientation tensors. (b) Visualization of the set of admissible planar fourth-order fiber orientation tensors $\mathcal{N}^{\text{planar}}$ in the parameter space $\{\lambda_1, d_1, d_8\}$ using the parameterization of $\mathbb{N}^{\text{planar}}$ in equation (15).

in Kelvin–Mandel [23–25] notation, which is explained in detail in Appendix 1. The Kelvin–Mandel basis $\mathbf{B}_\xi^v \otimes \mathbf{B}_\zeta^v$ is spanned in the orientation coordinate system $\{\mathbf{v}_i\}$, i.e., for example, the fourth basis vector in equation (78) becomes $\mathbf{B}_4^v = \sqrt{2}/2(\mathbf{v}_2 \otimes \mathbf{v}_3 + \mathbf{v}_3 \otimes \mathbf{v}_2)$. In equation (15), a short hand notation for completely symmetric fourth-order tensors following Bauer and Böhlke [13] is used, which is explained in Appendix 1. Demanding positive eigenvalues of $\mathbb{N}^{\text{planar}}$ in equation (15) leads to the set of admissible planar fourth-order orientation tensors

$$\mathcal{N}^{\text{planar}} = \left\{ \mathbb{N}^{\text{planar}}(\lambda_1, d_1, d_8) \mid \frac{1}{2} \leq \lambda_1 \leq 1, \quad -\frac{4}{35} \leq d_1 \leq -\frac{4}{35} + \lambda_1 - \lambda_1^2, \quad -f(\lambda_1, d_1) \leq d_8 \leq f(\lambda_1, d_1) \right\}, \quad (16)$$

with

$$f(\lambda_1, d_1) = \frac{1}{35} \sqrt{-16 - 280d_1 - 1225d_1^2 + 140\lambda_1 - 140\lambda_1^2 + 1225d_1\lambda_1 - 1225d_1\lambda_1^2}, \quad (17)$$

see [13, equation (89)]. The set $\mathcal{N}^{\text{planar}}$ implicitly defines a body in the parameter space $\{\lambda_1, d_1, d_8\}$. This body is visualized in Figure 1(b) and contains all admissible planar fourth-order fiber orientation tensors. Any point inside this body represents a fourth-order orientation tensor.

As Bauer and Böhlke [13] derive $\mathcal{N}^{\text{planar}}$ solely from algebraic properties of $\mathbb{N}^{\text{planar}}$, no planar fourth-order fiber orientation tensor outside $\mathcal{N}^{\text{planar}}$ exists. Consequently, the parameterization $\mathbb{N}^{\text{planar}}(\lambda_1, d_1, d_8)$ combined with the parameter space $\mathcal{N}^{\text{planar}}$ allows for a complete study of the influence of fiber orientation on the mechanical response of material models, which are based on fourth-order fiber orientation tensors of planar fiber architectures. However, not necessarily all points inside $\mathcal{N}^{\text{planar}}$ represent orientation states which differ structurally, and therefore lead to different mechanical behavior. Two tensors \mathbb{A} and \mathbb{B} are called structurally identical if they differ solely by a rotation, i.e.,

$$\exists \mathbf{Q} \in \text{SO}(3) \text{ with } \mathbf{Q} \star \mathbb{A} = \mathbb{B}, \quad (18)$$

holds with the special orthogonal group in three dimensions $\text{SO}(3)$. The parameterization of $\mathbb{N}^{\text{planar}}$ in equation (15) and the corresponding set of admissible parameter combinations $\mathcal{N}^{\text{planar}}$ in equation (16)

are based on the orientation coordinate system which is introduced in equations (10) to (12). However, for orientation states with planar isotropic second-order orientation tensor, i.e., $\lambda_1 = 1/2$, the eigenvalue problem identifying \mathbf{v}_1 and \mathbf{v}_2 is ill-posed. As the eigenvalues of $\mathbf{N}(\lambda_1 = 1/2)$ are $1/2, 1/2$, and 0 , any pair of two orthonormal vectors being pairwise perpendicular to \mathbf{v}_3 is a valid choice for the eigenvectors. The ambiguity of the orientation coordinate system introduces a redundancy in the set of admissible fourth-order orientation tensors given in equation (16), i.e., multiple parameter combinations lead to structurally identical $\mathbb{N}^{\text{planar}}$. The shape of the body $\mathcal{N}^{\text{planar}}$ in Figure 1(b) motivates the reparameterization of $\mathbb{N}^{\text{planar}}(\lambda_1, d_1, d_8)$ as a function of λ_1, \hat{r} , and $\hat{\beta}$ with

$$d_1 = \hat{d}_1 + \frac{1}{2} [\lambda_1 - \lambda_1^2] - \frac{4}{35}, \quad (19)$$

$$\hat{d}_1 = \hat{r} \sin(\hat{\beta}), \quad (20)$$

$$d_8 = \hat{r} \cos(\hat{\beta}). \quad (21)$$

The parameters \hat{r} and $\hat{\beta}$ are visualized in Figure 2(a) and lead to a reformulation of equation (15) with

$$\mathbb{N}^{\text{planar}}(\lambda_1, \hat{r}, \hat{\beta}) = \left[\begin{array}{ccc|ccc} -\hat{r} \sin(\hat{\beta}) + \frac{\lambda_1^2 + \lambda_1}{2} & \hat{r} \sin(\hat{\beta}) - \frac{\lambda_1^2 + \lambda_1}{2} & 0 & 0 & 0 & \sqrt{2}\hat{r} \cos(\hat{\beta}) \\ & -\hat{r} \sin(\hat{\beta}) + \frac{\lambda_1^2 + \lambda_1}{2} - \frac{3\lambda_1}{2} + 1 & 0 & 0 & 0 & -\sqrt{2}\hat{r} \cos(\hat{\beta}) \\ & & 0 & 0 & 0 & 0 \\ \hline & & & \text{completely} & & \text{symmetric} \end{array} \right] \mathbf{B}_\xi^v \otimes \mathbf{B}_\zeta^v, \quad (22)$$

and equation (16) by

$$\mathcal{N}^{\text{planar}} = \left\{ \mathbb{N}^{\text{planar}}(\lambda_1, \hat{r}, \hat{\beta}) \mid \frac{1}{2} \leq \lambda_1 \leq 1, 0 \leq \hat{r} \leq \frac{1}{2} [\lambda_1 - \lambda_1^2], 0 \leq \hat{\beta} < 2\pi \right\}. \quad (23)$$

For the special case $\lambda_1 = 1/2$, the reparameterized fourth-order fiber orientation tensor reads as

$$\mathbb{N}^{\text{planar}}(\lambda_1 = 1/2, \hat{r}, \hat{\beta}) = \left[\begin{array}{ccc|ccc} -\hat{r} \sin(\hat{\beta}) + \frac{3}{8} & \hat{r} \sin(\hat{\beta}) + \frac{1}{8} & 0 & 0 & 0 & \sqrt{2}\hat{r} \cos(\hat{\beta}) \\ & -\hat{r} \sin(\hat{\beta}) + \frac{3}{8} & 0 & 0 & 0 & -\sqrt{2}\hat{r} \cos(\hat{\beta}) \\ & & 0 & 0 & 0 & 0 \\ \hline & & & \text{completely} & & \text{symmetric} \end{array} \right] \mathbf{B}_\xi^v \otimes \mathbf{B}_\zeta^v, \quad (24)$$

and comparison with representations of rotations in the Kelvin–Mandel notation in Cowin and Mehrabadi [26, section 3] and Mehrabadi and Cowin [25, section 3] indicates a rotational redundancy. Active rotation of $\mathbb{N}^{\text{planar}}(\lambda_1 = 1/2, \hat{r}, \hat{\beta})$ by an angle of $-\hat{\beta}/4$ around the axis \mathbf{v}_3 leads to

$$\mathbf{Q}^{v_3}(\gamma = -\hat{\beta}/4) \star \mathbb{N}^{\text{planar}}(\lambda_1 = 1/2, \hat{r}, \hat{\beta}) = \mathbb{N}^{\text{planar}}(\lambda_1 = 1/2, \hat{r}, \hat{\beta} = 0), \quad (25)$$

$$= \left[\begin{array}{ccc|ccc} 3/8 & 1/8 & 0 & 0 & 0 & \sqrt{2}\hat{r} \\ & 3/8 & 0 & 0 & 0 & -\sqrt{2}\hat{r} \\ & & 0 & 0 & 0 & 0 \\ \hline & & & \text{completely} & & \text{symmetric} \end{array} \right] \mathbf{B}_\xi^v \otimes \mathbf{B}_\zeta^v,$$

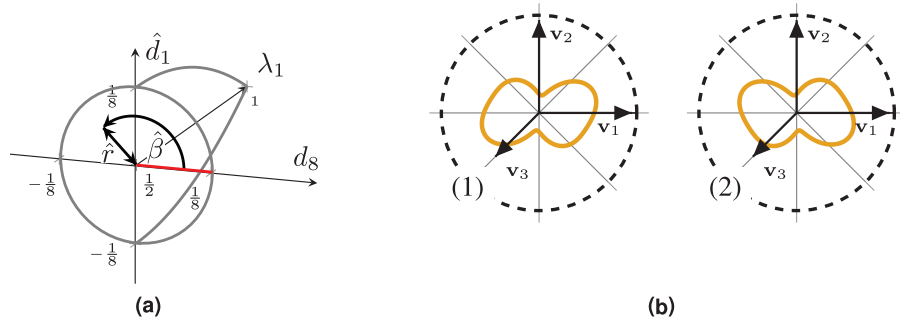


Figure 2. (a) The parameter space $\mathcal{N}^{\text{planar}}$ spanned by $(\lambda_1, \hat{d}_1, d_8)$ or equivalently $(\lambda_1, \hat{r}, \hat{\beta})$ following equations (19) to (21). The line $(\lambda_1 = 1/2, \hat{r}, 0)$ with $0 \leq \hat{r} \leq 1/8$ is colored in red. (b) As an example, an admissible parameter triplet (λ'_1, d'_1, d'_8) is randomly selected to be $(2/3, 1/[16\sqrt{2}], 1/[16\sqrt{2}])$. The polar plot (1) shows the projection of $\mathbb{N}^{\text{planar}}(\lambda'_1, d'_1, d'_8)$ onto the \mathbf{v}_1 – \mathbf{v}_2 –plane, i.e., $\mathbb{N}^{\text{planar}}(\lambda'_1, d'_1, d'_8) \cdot \mathbf{n}^{\otimes 4}(\varphi, \pi/2)$ with the fourth-order moment $\mathbf{n}^{\otimes 4}(\varphi, \theta)$ of a unit vector $\mathbf{n}(\varphi, \theta)$ in polar coordinates, e.g., defined in equation (33). The polar plot (2) shows $\mathbb{N}^{\text{planar}}(\lambda'_1, d'_1, -d'_8) \cdot \mathbf{n}^{\otimes 4}(\varphi, \pi/2)$.

with a rotation around the axis \mathbf{v}_3 parameterized by the angle γ with

$$\mathbf{Q}^{\mathbf{v}_3}(\gamma) = \begin{bmatrix} \cos(\gamma) & -\sin(\gamma) & 0 \\ \sin(\gamma) & \cos(\gamma) & 0 \\ 0 & 0 & 1 \end{bmatrix} \mathbf{v}_i \otimes \mathbf{v}_j. \quad (26)$$

As the angle $\hat{\beta}$ in equation (25) is arbitrary and the right-hand side of equation (25) is independent of $\hat{\beta}$, any $\mathbb{N}^{\text{planar}}(\lambda_1 = 1/2, \hat{r}, \hat{\beta})$ can be expressed by a reference tensor $\mathbb{N}^{\text{planar}}(\lambda_1 = 1/2, \hat{r}, \hat{\beta} = 0)$ combined with a rotation by

$$\mathbb{N}^{\text{planar}}(\lambda_1 = 1/2, \hat{r}, \hat{\beta}) = \mathbf{Q}^{\mathbf{v}_3}(\gamma = \hat{\beta}/4) \star \mathbb{N}^{\text{planar}}(\lambda_1 = 1/2, \hat{r}, \hat{\beta} = 0). \quad (27)$$

In consequence, coincidence or symmetry of the eigenvalues λ_1 and λ_2 in the special case of $\lambda_1 = 1/2$, degenerates the space of structurally differing planar fiber orientation tensors of fourth-order from a circle to a line. Fiber orientation tensors along this line act as reference tensors following equation (27). The line is, e.g., parameterized by \hat{r} or equivalently by d_8 and one arbitrary choice is colored red in Figure 2(a).

If $\mathbb{N}^{\text{planar}}$ serves as a directional measure, the full parameter range of d_8 , specified in equation (16), is necessary to account for all admissible orientation states. If, in contrast, the influence of $\mathbb{N}^{\text{planar}}$ onto mechanical properties or reconstructed FODF is to be studied, a minimal parameter set of structurally differing planar fiber orientation tensors is of interest. This set is given by

$$\hat{\mathcal{N}}^{\text{planar}} = \left\{ \mathbb{N}^{\text{planar}}(\lambda_1, d_1, d_8) \mid \frac{1}{2} < \lambda_1 \leq 1, -\frac{4}{35} \leq d_1 \leq -\frac{4}{35} + \lambda_1 - \lambda_1^2, 0 \leq d_8 \leq f(\lambda_1, d_1) \right\}, \quad (28)$$

$$\cup \left\{ \mathbb{N}^{\text{planar}}(\lambda_1 = 1/2, d_1, d_8) \mid d_1 = 0, 0 \leq d_8 \leq 1/8 \right\},$$

with $\mathbb{N}^{\text{planar}}$ and $f(\lambda_1, d_1)$ defined in equations (15) and (17) and $f(\lambda_1 = 1/2, d_1 = 0) = 1/8$. Equation (28) accounts for the special case $\lambda_1 = 1/2$ and removes a second redundancy which is visualized in Figure 2(b) and derived by the following observation. Two fiber orientation tensors of fourth order $\mathbb{N}^{\text{planar}}(\lambda_1, d_1, d_8)$ which differ solely by the sign of the parameter d_8 are structurally identical and only differ by the rotation

$$\mathbf{Q}^{\text{monox}} = \begin{bmatrix} 1 & 0 & 0 \\ 0 & -1 & 0 \\ 0 & 0 & -1 \end{bmatrix} \mathbf{v}_i \otimes \mathbf{v}_j, \quad (29)$$

which rotates any physical quantity by 180° around the axis \mathbf{v}_1 . Due to its symmetries, for any planar fourth-order fiber orientation tensor

$$\mathbf{Q}^{\text{monox}} \star \mathbb{N}^{\text{planar}}(\lambda_1, d_1, d_8) = \mathbb{N}^{\text{planar}}(\lambda_1, d_1, -d_8), \quad (30)$$

holds and motivates restriction to positive values of d_8 in the minimal set specified in equation (28). This set can be used to study the influence of planar fourth-order orientation tensors on derived quantities.

2.3. Reconstructed FODF

In the previous section, distinct and admissible planar fiber orientation tensors of fourth order are identified. The question of interest is, which fiber orientation distributions are associated with these tensors? It is evident from equation (13) that for a given leading fiber orientation tensor, there is non one-to-one correspondence to an FODF. However, identification of any FODF which is connected to the given leading fiber orientation tensor is of interest. An approximation of an FODF by leading fiber orientation tensors up to fourth order in a 3D framework is given by

$$\hat{\psi}(\mathbf{n}, \mathbb{N}) = \frac{1}{4\pi} \left[1 + \frac{15}{2} \text{dev}(\mathbb{N}) \cdot \mathbf{n}^{\otimes 2} + \frac{315}{8} \text{dev}(\mathbb{N}) \cdot \mathbf{n}^{\otimes 4} \right], \quad (31)$$

following equation (13), where \mathbf{N} can be expressed by \mathbb{N} based on equation (8). Müller and Böhlke [14] discuss that the approximation $\hat{\psi}(\mathbf{n}, \mathbb{N})$ is not necessarily non-negative, i.e., the condition stated on $\psi(\mathbf{n})$ in equation (2) does not hold for the approximation $\hat{\psi}(\mathbf{n}, \mathbb{N})$, due to the truncation after the fourth-order term. For the special case of planar fiber orientation tensors $\mathbb{N}^{\text{planar}}$, the approximation in equation (31) leads to

$$\begin{aligned} \hat{\psi}^{\mathbb{N}^{\text{planar}}}(\varphi, \theta, \lambda_1, d_1, d_8) &= \hat{\psi}(\mathbf{n}(\varphi, \theta), \mathbb{N}^{\text{planar}}(\lambda_1, d_1, d_8)), \\ &= \frac{1}{2048\pi} [20160d_8 \sin^4(\theta) \sin(4\varphi) + 3[72 - 6720d_1] \sin^4(\theta) \cos(4\varphi), \\ &\quad - 3[1120\lambda_1 - 560][3 \cos(2\theta) + 1] \sin^2(\theta) \cos(2\varphi) - 420 \cos(2\theta), \\ &\quad + 945 \cos(4\theta) + 435], \end{aligned} \quad (32)$$

with a parameterization of the unit vector \mathbf{n} in two spherical angles

$$\mathbf{n}(\varphi, \theta) = \sin(\theta) \cos(\varphi) \mathbf{v}_1 + \sin(\theta) \sin(\varphi) \mathbf{v}_2 + \cos(\theta) \mathbf{v}_3. \quad (33)$$

The approximation $\hat{\psi}^{\mathbb{N}^{\text{planar}}}$ is not planar. Figure 3(a) to (c) shows three-dimensional spherical plots of $\hat{\psi}^{\mathbb{N}^{\text{planar}}}(\theta, \varphi, \lambda_1, d_1, d_8)$ for three selected combinations of the parameters λ_1 , d_1 , and d_8 . Representation of non-smooth functions by the Fourier series requires an infinite number of non-vanishing Fourier coefficients. For any given planar FODF, the transition from non-vanishing values in the plane spanned by \mathbf{v}_1 and \mathbf{v}_2 , to vanishing values outside this plane is not smooth. In consequence, this transition is inadequately represented by the truncated spherical Fourier series $\hat{\psi}^{\mathbb{N}^{\text{planar}}}$. As a result, planarity of a given fiber orientation tensor in a 3D framework does not imply that derived quantities, such as reconstructed FODF, are planar as well. Following Bauer and Böhlke [13, equation (59)], any fourth-order fiber orientation tensor in three dimensions can be expressed by two deviators $\text{dev}(\mathbf{N})$ and $\text{dev}(\mathbb{N})$ fulfilling

$$\mathbb{N} = \mathbb{N}^{\text{iso}} + \frac{6}{7} \text{sym}(\text{dev}(\mathbb{N}[\mathbf{I}]) \otimes \mathbf{I}) + \text{dev}(\mathbb{N}). \quad (34)$$

Vanishing deviators, i.e., $\text{dev}(\mathbf{N}) = 0$ and $\text{dev}(\mathbb{N}) = 0$ describe the isotropic state $\mathbb{N}^{\text{iso}} = (7/35) \text{sym}(\mathbf{I} \otimes \mathbf{I})$ which corresponds to the FODF $\psi(\mathbf{n}, \mathbb{N}^{\text{iso}}) = 1/(4\pi)$ and which is not planar. For $\mathbb{N}^{\text{planar}}$, the deviators from the isotropic state which are also utilized in equation (31) read as

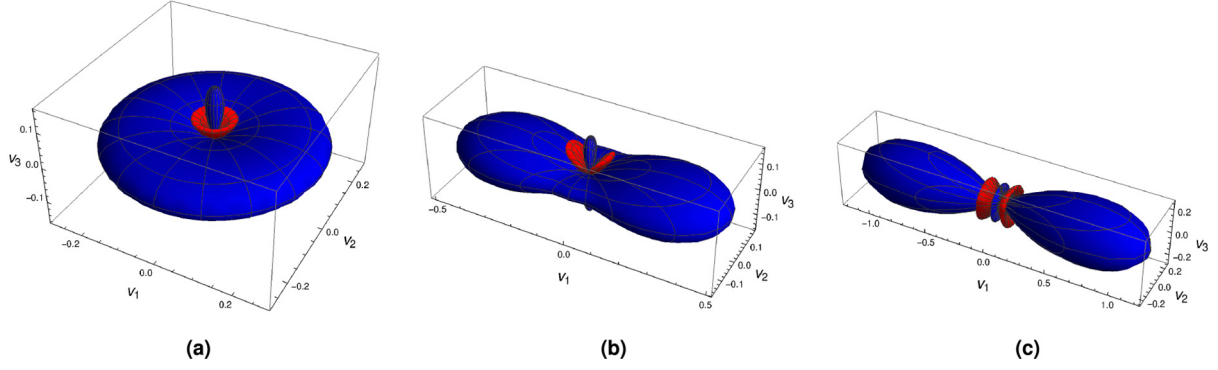


Figure 3. Approximation of the FODF by leading fiber orientation tensors up to fourth-order following equation (32), i.e., $\hat{\psi}_{\mathbb{N}^{\text{planar}}}(\varphi, \theta, \mathbb{N}^{\text{planar}}(\lambda_1, d_1, d_8))$ for three selected points in $\mathcal{N}^{\text{planar}}$. Positive values are plotted in blue and negative values are plotted in red. The parameters in the format (λ_1, d_1, d_8) are (a) $(1/2, 3/280, 0)$ (b) $(2/3, -1/315, 0)$, and (c) $(1, -4/35, 0)$.

$$\text{dev}(\mathbb{N}^{\text{planar}}) = \begin{bmatrix} \lambda_1 - 1/3 & 0 & 0 \\ \text{sym} & 2/3 - \lambda_1 & 0 \\ & & -1/3 \end{bmatrix} \mathbf{v}_i \otimes \mathbf{v}_j, \quad (35)$$

$$\text{dev}(\mathbb{N}^{\text{planar}}) = \left[\begin{array}{ccc|ccc} \lambda_1/7 - d_1 - \frac{1}{35} & d_1 & 1/35 - \lambda_1/7 & 0 & 0 & \sqrt{2}d_8 \\ & (1 - \lambda_1)/7 - d_1 - 1/35 & 1/35 - (1 - \lambda_1)/7 & 0 & 0 & -\sqrt{2}d_8 \\ & & 3/35 & 0 & 0 & 0 \\ \hline & \text{completely} & & & \text{symmetric} & \end{array} \right] \mathbf{B}'_{\xi} \otimes \mathbf{B}'_{\zeta}, \quad (36)$$

and demonstrate the drawbacks of expressing planar fiber orientation tensors in a 3D framework since the planarity has to be enforced by deviation from the isotropic state. Note that the fourth-order deviator depends on the parameter λ_1 which defines the second-order fiber orientation tensor.

2.3.1. Transition from 3D into 2D. Motivated by the previous section and following [1,27–30], planar quantities are expressed in a 2D framework with representations

$$\mathbf{a} = \sum_{i=1}^2 a_i \mathbf{e}_i = \underline{a}_1 \mathbf{e}_1 + \underline{a}_2 \mathbf{e}_2 + 0 \mathbf{e}_3, \quad (37)$$

$$\underline{\mathbf{A}} = \sum_{i=1}^2 \sum_{j=1}^2 \underline{A}_{ij} \mathbf{e}_i \otimes \mathbf{e}_j = \sum_{i=1}^2 \sum_{j=1}^2 \underline{A}_{ij} \mathbf{e}_i \otimes \mathbf{e}_j + \sum_{i=1}^3 0 \mathbf{e}_i \otimes \mathbf{e}_3 + \sum_{j=1}^3 0 \mathbf{e}_3 \otimes \mathbf{e}_j, \quad (38)$$

$$\underline{\underline{\mathbf{A}}} = \sum_{\xi=1}^3 \sum_{\zeta=1}^3 \underline{\underline{A}}_{\xi\zeta} \mathbf{B}_{\xi} \otimes \mathbf{B}_{\zeta} = \sum_{\xi \in [1, 2, 4]}^3 \sum_{\zeta \in [1, 2, 4]}^3 \underline{\underline{A}}_{\xi\zeta} \mathbf{B}_{\xi} \otimes \mathbf{B}_{\zeta}, \quad (39)$$

with generic tensors \mathbf{a} , $\underline{\mathbf{A}}$, and $\underline{\underline{\mathbf{A}}}$. This notation directly connects objects in \mathbb{R}^2 and \mathbb{R}^3 and requires the reader to select the appropriate two-dimensional or three-dimensional view onto the planar physical quantity of interest, which is part of the three-dimensional reality. For the two-dimensional Kelvin–Mandel bases, $\underline{\mathbf{B}}_1 = \mathbf{B}_1$, $\underline{\mathbf{B}}_2 = \mathbf{B}_2$, and $\underline{\mathbf{B}}_3 = \mathbf{B}_4$ hold. To be explicit, for indices of tensor components in the 2D framework $i, j \in [1, 2]$ and $\xi, \zeta \in [1, 2, 3]$ hold in contrast to $i, j \in [1, 2, 3]$ and $\xi, \zeta \in [1, 2, 3, 4, 5, 6]$ in the 3D framework.

If planar orientation tensors are derived from a 2D framework, naturally no out-of-plane tensor components exist. Basic planar isotropic tensors in the 2D framework are given by

$$\mathbf{I} = \delta_{ij} \mathbf{e}_i \otimes \mathbf{e}_j = \begin{bmatrix} 1 & 0 \\ \text{sym} & 1 \end{bmatrix} \mathbf{e}_i \otimes \mathbf{e}_j, \quad \mathbb{I}^S = \delta_{\xi\xi} \mathbf{B}_\xi \otimes \mathbf{B}_\xi = \begin{bmatrix} 1 & 0 & 0 \\ & 1 & 0 \\ \text{sym} & & 1 \end{bmatrix} \mathbf{B}_\xi \otimes \mathbf{B}_\xi, \quad (40)$$

$$\mathbb{P}_1 = \frac{1}{2} \mathbf{I} \otimes \mathbf{I}, \quad \mathbb{P}_2 = \mathbb{I}^S - \mathbb{P}_1, \quad (41)$$

following Blinowski et al. [27, equation (2.3)] and Aßmus et al. [31, equation (38)]. Deviator operators are defined by

$$\text{dev}(\underline{\mathbf{A}}) = \underline{\mathbf{A}} - \frac{1}{2} (\underline{\mathbf{A}} \cdot \mathbf{I}) \mathbf{I}, \quad (42)$$

$$\text{dev}(\underline{\mathbb{A}}) = \text{sym}(\underline{\mathbb{A}}) - \text{sym}(\text{sym}(\underline{\mathbb{A}}) [\mathbf{I} \otimes \mathbf{I}]) + \frac{1}{8} \text{sym}(\mathbf{I} \otimes \mathbf{I}) (\mathbf{I} \cdot \underline{\mathbb{A}} \mathbf{I}), \quad (43)$$

following Kanatani [1, (7.13)] and Vianello [28, section 3]. The central fiber orientation tensor in the 2D framework is identified as

$$\begin{aligned} \underline{\mathbb{N}}^{\text{piso}} &= \left(\frac{\mathbb{P}_1}{\|\mathbb{P}_1\|} \cdot \mathbf{n}^{\otimes 4} \right) \mathbb{P}_1 + \left(\frac{\mathbb{P}_2}{\|\mathbb{P}_2\|} \cdot \mathbf{n}^{\otimes 4} \right) \mathbb{P}_2 = \frac{1}{2} \mathbb{P}_1 + \frac{1}{4} \mathbb{P}_2, \\ &= \frac{1}{8} \left[\begin{array}{cc|c} 3 & 1 & 0 \\ & 3 & 0 \\ \hline \text{compl.} & & \text{sym.} \end{array} \right] \mathbf{B}_\xi \otimes \mathbf{B}_\xi = \mathbb{N}^{\text{planar}}(\lambda_1 = 1/2, d_1 = 0, d_8 = 0), \end{aligned} \quad (44)$$

and is called planar isotropic fiber orientation tensor of fourth order. It should be noted that this is not the only fourth-order fiber orientation tensor which contracts to the planar isotropic second-order fiber orientation tensor. Deploying harmonic decomposition in the 2D framework following Blinowski et al. [27, equation (2.25)] or Desmorat and Desmorat [29, equation (18)] with

$$\underline{\mathbb{A}} = \left(\frac{\mathbb{P}_1}{\|\mathbb{P}_1\|} \cdot \underline{\mathbb{A}} \right) \mathbb{P}_1 + \left(\frac{\mathbb{P}_2}{\|\mathbb{P}_2\|} \cdot \underline{\mathbb{A}} \right) \mathbb{P}_2 + \text{sym}(\text{dev}(\underline{\mathbb{A}} \mathbf{I}) \otimes \mathbf{I}) + \text{dev}(\underline{\mathbb{A}}), \quad (45)$$

and knowledge on irreducible tensors, any fourth-order fiber orientation tensor is parameterized by

$$\underline{\mathbb{N}}(\lambda_1, p_1, p_2) = \underline{\mathbb{N}}^{\text{piso}} + \text{sym}(\underline{\mathbf{F}}(\lambda_1) \otimes \mathbf{I}) + \underline{\mathbb{F}}(p_1, p_2), \quad (46)$$

with

$$\underline{\mathbf{F}}(\lambda_1) = \left(\lambda_1 - \frac{1}{2} \right) \begin{bmatrix} 1 & 0 \\ \text{sym} & -1 \end{bmatrix} \mathbf{v}_i \otimes \mathbf{v}_j, \quad (47)$$

$$\underline{\mathbb{F}}(p_1, p_2) = \left(p_1 \left[\begin{array}{cc|c} -1 & 1 & 0 \\ & -1 & 0 \\ \hline \text{compl.} & & \text{sym.} \end{array} \right] + p_2 \left[\begin{array}{cc|c} 0 & 0 & \sqrt{2} \\ & 0 & -\sqrt{2} \\ \hline \text{compl.} & & \text{sym.} \end{array} \right] \right) \mathbf{B}_\xi^v \otimes \mathbf{B}_\xi^v. \quad (48)$$

Coincidence with the parameterization in the 3D framework is given by the prefactor in equation (47) and the specific choice of the factors $p_1 = d_1 - 3/280$ and $p_2 = d_8$ leading to

$$\underline{\mathbb{N}}(\lambda_1, d_1, d_8) = \left[\begin{array}{cc|c} \lambda_1 - d_1 - 4/35 & d_1 + 4/35 & \sqrt{2}d_8 \\ & (1 - \lambda_1) - d_1 - 4/35 & -\sqrt{2}d_8 \\ \hline & \text{compl.} & \text{sym.} \end{array} \right] \mathbf{B}_\xi^v \otimes \mathbf{B}_\zeta^v. \quad (49)$$

The shift by $3/280$ is required due to the different expansion points in 2D and 3D. As the point of expansion in equation (46), i.e., $\underline{\mathbb{N}}^{\text{piso}}$, is planar itself, the deviators are compact and formatted into the 3D framework read as

$$\text{dev}(\underline{\mathbb{N}}) = \left[\begin{array}{ccc|c} \lambda_1 - 1/2 & 0 & 0 & \mathbf{v}_i \otimes \mathbf{v}_j \\ & 1/2 - \lambda_1 & 0 & \\ \hline \text{sym} & & 0 & \end{array} \right] \quad (50)$$

$$\text{dev}(\underline{\mathbb{N}}) = \left[\begin{array}{ccc|ccc} \frac{3}{280} - d_1 & -(\frac{3}{280} - d_1) & 0 & 0 & 0 & \sqrt{2}d_8 \\ & \frac{3}{280} - d_1 & 0 & 0 & 0 & -\sqrt{2}d_8 \\ & & 0 & 0 & 0 & 0 \\ \hline & \text{completely} & & \text{symmetric} & & \end{array} \right] \mathbf{B}_\xi^v \otimes \mathbf{B}_\zeta^v. \quad (51)$$

The deviators specified in equations (35), (36), (50), and (51) directly enter approximations of the FODF in terms of truncated Fourier series.

2.3.2. Truncated fiber orientation distribution function in the 2D framework. In analogy to the three-dimensional case in equation (13), FODF can be reconstructed in a two-dimensional framework. An FODF is given in terms of fiber orientation tensors by a tensorial Fourier series [1, p. 158]

$$\underline{\psi}(\underline{\mathbf{n}}) = \frac{1}{2\pi} \sum_{k=0}^{\infty} 2^k \text{dev}(\underline{\mathbb{N}}_{<k>}) \cdot \underline{\mathbf{n}}^{\otimes k}, \quad (52)$$

with a unit tensor of first order $\underline{\mathbf{n}}$ and fiber orientation tensors of k th order in two dimensions $\underline{\mathbb{N}}_{<k>}$. An approximation of the FODF $\underline{\psi}(\underline{\mathbf{n}})$ by leading fiber orientation tensors up to fourth order is given by

$$\hat{\underline{\psi}}(\underline{\mathbf{n}}, \underline{\mathbb{N}}) = \frac{1}{2\pi} [1 + 4 \text{dev}(\underline{\mathbb{N}}) \cdot \underline{\mathbf{n}}^{\otimes 2} + 16 \text{dev}(\underline{\mathbb{N}}) \cdot \underline{\mathbf{n}}^{\otimes 4}], \quad (53)$$

and combined with $\underline{\mathbb{N}}(\lambda_1, p_1, p_2)$ and $\underline{\mathbf{n}}(\varphi) = \cos(\varphi) \mathbf{v}_1 + \sin(\varphi) \mathbf{v}_2$ leads to

$$\hat{\underline{\psi}}(\varphi, \lambda_1, p_1, p_2) = \frac{1}{2\pi} [1 + (4\lambda_1 - 2) \cos(2\varphi) - 16p_1 \cos(4\varphi) + 16p_2 \sin(4\varphi)]. \quad (54)$$

Introducing the coordinate transformation

$$p_1 = \hat{r} \sin(\hat{\beta}), \quad p_2 = \hat{r} \cos(\hat{\beta}), \quad (55)$$

yields the following formulation

$$\hat{\underline{\psi}}(\varphi, \lambda_1, \hat{r}, \hat{\beta}) = \frac{1}{2\pi} \left[1 + 4 \left(\lambda_1 - \frac{1}{2} \right) \cos(2\varphi) - 16\hat{r} \sin(\hat{\beta} - 4\varphi) \right]. \quad (56)$$

The parameterization of $\hat{\underline{\psi}}$ in equation (56) separates second- and fourth-order contributions into one trigonometric summand each. The cosine contribution of the second-order fiber orientation tensor is always aligned with the coordinate axes of the orientation coordinate system and its amplitude scales with λ_1 , being zero for the planar isotropic case, i.e., $\lambda_1 = 1/2$ and the frequency is two in the interval $\varphi \in [0, 2\pi)$. The fourth-order summand is a sinusoidal function of double the frequency of the second-

order term, with phase shift $\hat{\beta}$ and an amplitude which scales with \hat{r} . The frequency implies that this fourth-order term has four maxima and four minima within the parameter range of $\varphi \in [0, 2\pi)$. In consequence, in the planar isotropic case, equation (56) degenerates to

$$\hat{\underline{\psi}}\left(\varphi, \lambda_1 = \frac{1}{2}, \hat{r}, \hat{\beta}\right) = \frac{1}{2\pi} \left[1 - 16\hat{r} \sin\left(\hat{\beta} - 4\varphi\right) \right], \quad (57)$$

which directly indicates that the parameter $\hat{\beta}$ implies a rotation of $\hat{\underline{\psi}}$ by an angle of $\hat{\beta}/4$ around the axis \mathbf{v}_3 of the 3D framework pointing out of the 2D plane. If $\lambda_1 \neq 1/2$, the interference of the second- and fourth-order summands, which have different frequencies, leads to the variety of $\hat{\underline{\psi}}$. The structure of equation (56) shows that $\hat{\underline{\psi}}$ may be represented by circular harmonics. Further details on harmonic representations of planar tensors of fourth-order can be found, e.g., in Vannucci [30, Chapter 4] and Forte and Vianello [32].

2.3.3. Maximum entropy reconstruction of the FODF. Identification of a representative FODF based on a given leading fiber orientation tensor is of importance for several applications, e.g., numerical calculation of orientation averages of direction dependent mechanical properties [8,9,12]. Truncated Fourier series are used in literature to identify an FODF based on fiber orientation tensors [6,33] although the identified functions do not meet the non-negativity requirement of an FODF. Naive averaging with partly negative FODF leads to non-physical results. Müller and Böhlke [14] give a solution to the reconstruction problem and identify FODF based on leading fiber orientation tensors by maximizing the information-theoretic entropy fulfilling normalization and non-negativity constraints. For limited available information, the entropy principle yields the most likely FODF fulfilling specified constraints. In this context, “most likely” corresponds to “maximizing entropy.” The procedure of Müller and Böhlke [14] is briefly repeated for the special case of fourth-order fiber orientation tensors and tailored to planar fiber orientation tensors. The maximum entropy approximation $\hat{\underline{\psi}}^{\text{me}}(\mathbf{n})$ maximizes the information-theoretic entropy $E(\hat{\underline{\psi}})$

$$E(\hat{\underline{\psi}}) = - \int_{S^{n-1}} \hat{\underline{\psi}}(\mathbf{n}) \ln \hat{\underline{\psi}}(\mathbf{n}) dS, \quad (58)$$

and fulfills the constraints

$$G = \mathbb{G}_{\langle 0 \rangle} = - \int_{S^{n-1}} \hat{\underline{\psi}}(\mathbf{n}) dS - 1, \quad (59)$$

$$\mathbf{G} = \mathbb{G}_{\langle 2 \rangle} = - \int_{S^{n-1}} \hat{\underline{\psi}}(\mathbf{n}) \text{dev}(\mathbf{n}^{\otimes 2}) dS - \text{dev}(\mathbf{N}), \quad (60)$$

$$\mathbb{G} = \mathbb{G}_{\langle 4 \rangle} = - \int_{S^{n-1}} \hat{\underline{\psi}}(\mathbf{n}) \text{dev}(\mathbf{n}^{\otimes 4}) dS - \text{dev}(\mathbb{N}), \quad (61)$$

where the constraint G ensures the normalization, and \mathbf{G} and \mathbb{G} ensure that the solution $\hat{\underline{\psi}}^{\text{me}}(\mathbf{n})$ meets the given orientation tensors. The domain of the integral depends on the dimensionality of the given orientation tensor and is either the surface of the unit sphere S^2 for planar 3D tensors or the circumference of the unit circle S^1 for 2D tensors. The problem

$$\max_{\hat{\underline{\psi}}} E(\hat{\underline{\psi}}) \quad \text{with} \quad \mathbb{G}_{\langle \alpha \rangle} = 0_{\langle \alpha \rangle} \quad \text{for} \alpha \in [0, 2, 4], \quad (62)$$

corresponds to the Lagrange functional

$$\mathcal{L}(\hat{\underline{\psi}}) = E(\hat{\underline{\psi}}) - \sum_{\alpha \in [0, 2, 4]} \mathbb{L}_{\langle \alpha \rangle} \cdot \mathbb{G}_{\langle \alpha \rangle}, \quad (63)$$

Table 1. Number of independent components of irreducible tensors depending on order and dimensionality of the vector space.

Tensor order	2D	3D
2	2	5
4	2	9

with Lagrange multipliers $L = \mathbb{L}_{\langle 0 \rangle}$, $\mathbf{L} = \mathbb{L}_{\langle 2 \rangle}$, and $\mathbb{L} = \mathbb{L}_{\langle 4 \rangle}$. The solution is given by the root of the first variation of \mathcal{L} , i.e., $\delta\mathcal{L}(\hat{\psi}) = 0$ and is formulated in the Lagrange multipliers by

$$\hat{\psi}^{\text{me}}(\mathbf{n}, L, \mathbf{L}, \mathbb{L}) = \exp(-1 - L - \mathbf{L} \cdot \text{dev}(\mathbf{n}^{\otimes 2}) - \mathbb{L} \cdot \text{dev}(\mathbf{n}^{\otimes 4})), \quad (64)$$

which fulfills the non-negativity condition identically. The Lagrange multipliers are obtained by solving the system of equations stated by the constraints in equations (59) to (61), with $\hat{\psi}(\mathbf{n})$ being replaced by $\hat{\psi}^{\text{me}}(\mathbf{n}, L, \mathbf{L}, \mathbb{L})$ from equation (64). Due to the projection of the Lagrange multipliers onto deviators of the moment tensors in equation (64), the Lagrange multipliers are without loss generality irreducible, i.e., completely symmetric and traceless [21,34]. Table 1 lists the number of independent components of irreducible tensors which depend on the tensor order and the dimensionality of the vector space. The number of independent components of the Lagrange multipliers L , \mathbf{L} , and \mathbb{L} sum up to $1 + 5 + 9 = 15$ and $1 + 2 + 2 = 5$ in three and two dimensions, respectively, and correspond to the fourteen independent components of \mathbb{N} and four independent components of $\underline{\mathbb{N}}$ plus one normalization constraint each. In tensor notation, equations (59) to (61) read as $1 + 9 + 81 = 91$ scalar equations, whereas in symmetric Kelvin–Mandel notation, the identical equations yield $1 + 6 + 36$ scalar equations. These naive views on the set of equations illustrate that a minimal and redundancy-free parameterization deploying index symmetry of the Lagrange multipliers is required. Such a parameterization is necessary to reduce the dimensionality of the system of equations to at most 15 or 5 depending on the dimensionality of used tensor framework. Three out of five independent components of \mathbf{N} in 3D and one out of two independent components of $\underline{\mathbf{N}}$ in 2D define the orientation coordinate system. In the orientation coordinate system, the second-order orientation tensor has diagonal structure. Off-diagonal components of the second-order Lagrange multiplier ensure that the orientation coordinate systems of the reconstructed FODF and the original fiber orientation tensors coincide. Based on the orientation coordinate system, a generic representation of the Lagrange multipliers of order two and four in three dimensions is given by

$$\mathbf{L}(b_1, \dots, b_5) = \begin{bmatrix} b_1 & b_5 & b_4 \\ & b_2 & b_3 \\ \text{sym} & & -(b_1 + b_2) \end{bmatrix} \mathbf{v}_i \otimes \mathbf{v}_j, \quad (65)$$

$$\mathbb{L}(c_1, \dots, c_9) = \left[\begin{array}{ccc|ccc} -(c_1 + c_2) & c_1 & c_2 & -\sqrt{2}(c_4 + c_5) & \sqrt{2}c_6 & \sqrt{2}c_8 \\ & -(c_1 + c_3) & c_3 & \sqrt{2}c_4 & -\sqrt{2}(c_6 + c_7) & \sqrt{2}c_9 \\ & & -(c_2 + c_3) & \sqrt{2}c_5 & \sqrt{2}c_7 & -\sqrt{2}(c_8 + c_9) \\ \hline & \text{completely} & & & \text{symmetric} & \end{array} \right] \mathbf{B}_\xi^v \otimes \mathbf{B}_\zeta^v. \quad (66)$$

Starting from the triclinic case in equations (65) and (66), material symmetries may be deployed to further reduce the number of independent components of the Lagrange multipliers, as the fiber orientation tensors and the reconstructed FODF share their symmetry group, i.e., $\mathcal{S}^\psi = \mathcal{S}^{\mathbb{N}}$ with

$$\hat{\psi}(\mathbf{Q}\star\mathbf{n}) = \hat{\psi}(\mathbf{n}) \quad \forall \mathbf{Q} \in \mathcal{S}^\psi, \quad (67)$$

$$\mathbf{Q} \star \mathbb{N} = \mathbb{N} \quad \forall \mathbf{Q} \in \mathcal{S}^{\mathbb{N}}, \quad (68)$$

which follows directly from the definition of \mathbb{N} in equation (7). Similar to the FODF reconstruction by truncated Fourier series, the ansatz $\hat{\psi}^{\text{me}}$ in equation (64) contains deviators from a central state, which in 3D is the isotropic state. In order to reconstruct planar FODF based on planar fiber orientation tensors, it is beneficial to deploy a 2D framework with deviators deviating from the planar isotropic state. In the orientation coordinate system, the Lagrange multipliers of order two and four read as

$$\underline{\mathbf{L}}(f_1, f_2) = \begin{bmatrix} f_1 & f_2 \\ \text{sym} & -f_1 \end{bmatrix} \mathbf{v}_i \otimes \mathbf{v}_j, \quad (69)$$

$$\underline{\mathbf{L}}(g_1, g_2) = \left[\begin{array}{cc|c} -g_1 & g_1 & \sqrt{2}g_2 \\ & -g_1 & -\sqrt{2}g_2 \\ \text{compl.} & & \text{sym.} \end{array} \right] \mathbf{B}_\xi^{\mathbf{v}} \otimes \mathbf{B}_\xi^{\mathbf{v}}. \quad (70)$$

In consequence, combination of equations (69) and (70) leads to

$$\hat{\psi}^{\text{me}}(\varphi, L, f_1, f_2, g_1, g_2) = \exp(-1 - L - f_1 \cos(2\varphi) - f_2 \sin(2\varphi) + g_1 \cos(4\varphi) - g_2 \sin(4\varphi)). \quad (71)$$

For a given $\underline{\mathbf{N}}(\lambda_1, d_1, d_8)$ following equation (49) and a specific selection of independent tensor components, the resulting five scalar equations are

$$\int_{S^1} \hat{\psi}(\mathbf{n}, L, f_1, f_2, g_1, g_2) \, dS - 1 = 0, \quad (72)$$

$$\int_{S^1} \hat{\psi}(\mathbf{n}, L, f_1, f_2, g_1, g_2) \left(\frac{1}{2} \cos(2\varphi) \right) \, dS - \left(\lambda_1 - \frac{1}{2} \right) = 0, \quad (73)$$

$$\int_{S^1} \hat{\psi}(\mathbf{n}, L, f_1, f_2, g_1, g_2) \left(\frac{1}{2} \sin(2\varphi) \right) \, dS - 0 = 0, \quad (74)$$

$$\int_{S^1} \hat{\psi}(\mathbf{n}, L, f_1, f_2, g_1, g_2) \left(-\frac{1}{8} \cos(4\varphi) \right) \, dS - \left(d_1 - \frac{3}{280} \right) = 0, \quad (75)$$

$$\int_{S^1} \hat{\psi}(\mathbf{n}, L, f_1, f_2, g_1, g_2) \left(\frac{\sqrt{2}}{8} \sin(4\varphi) \right) \, dS - \sqrt{2}d_8 = 0. \quad (76)$$

The equations are solved numerically for a given tripled (λ_1, d_1, d_8) . Numerical integration on the unit circle is done with nschloe [35] based on Krylov and Stroud [36].

2.3.4. Visualization of reconstructed planar fiber orientation distribution functions. Fiber orientation tensors represent averaged properties of an underlying FODF. In consequence, a complete reconstruction of the underlying FODF is not possible. It is of interest to visualize possible shapes of reconstructed FODFs based on admissible mean values. The admissible mean values are given by the set of distinct and admissible fiber orientation tensors of fourth-order $\mathcal{N}^{\text{planar}}$ which can be combined with the developed reconstruction methods $\hat{\psi}$ and $\hat{\psi}^{\text{me}}$. The parameter space $\mathcal{N}^{\text{planar}}$ is discretized and for selected points in $\mathcal{N}^{\text{planar}}$, i.e., for selected $\underline{\mathbf{N}}$, reconstructed FODFs are visualized. The discretization is based on several slices through $\mathcal{N}^{\text{planar}}$ which are given in Figures 4 and 6(a). The arrangement of the visualizations of the reconstructed FODFs in Figures 6 and 7 mimics the position of the points on the slices and reuses the color coding of the overview plots. In consequence, the influence of the position inside $\mathcal{N}^{\text{planar}}$ on the shape of the reconstructed FODF is obtained. The developed visualizations directly show the variety of reconstructed FODFs and as a side effect acts as an intuitive view on fiber orientation tensors of fourth order. As the truncated FODF reconstruction does not fulfill the non-negativity constraint, negative values of $\hat{\psi}$ are highlighted in red, as defined in the shared legend in Figure 5. Parameters of the utilized orientation

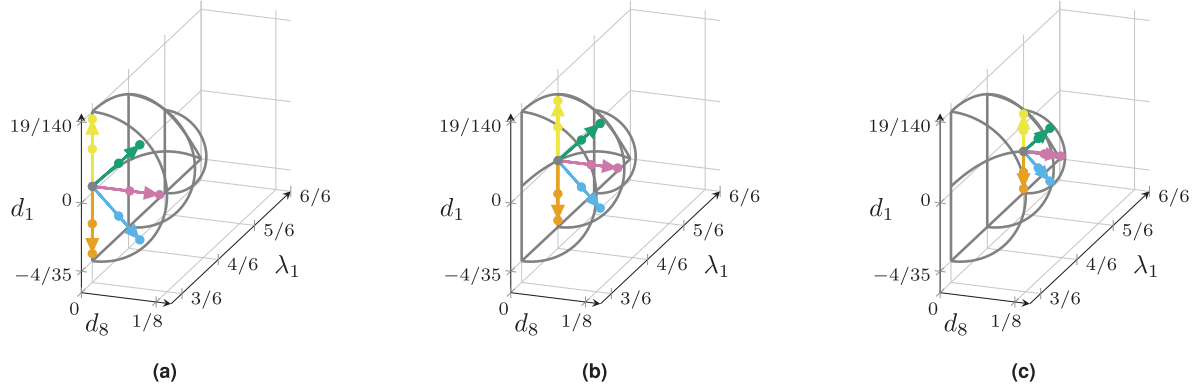


Figure 4. Definition of representative points in the parameter space $\hat{\mathcal{N}}^{\text{planar}}$ of planar fourth-order fiber orientation tensors. The outer points in radial directions do not lie on the boundary of the admissible region. Parameters of each point are listed in Table 2 in Appendix 2. (a) Paths and points in the plane $\lambda_1 = 3/6$ used in Figure 6(c). (b) Points in the plane $\lambda_1 = 4/6$ used in Figure 7(a). (c) Points in the plane $\lambda_1 = 5/6$ used in Figure 7(b).

— Positive values of $\hat{\psi}(\varphi)$ — Negative values of $\hat{\psi}(\varphi)$ $\hat{\psi}^{\text{me}}(\varphi)$

Figure 5. Shared legend for Figures 6(b), 7(a) and 7. $\hat{\psi}(\varphi)$ and $\hat{\psi}^{\text{me}}(\varphi)$ are defined in equations (53) and (71), respectively.

tensors are listed in Table 2 in Appendix 2. The scaling of all polar plots of FODFs in Figures 6(b) and (c) and 7 is homogeneous, with the lower radial limit being zero and the upper radial limit being 0.9.

A slice containing orthotropic [13] fiber orientation tensors is shown in Figure 6(a) and the corresponding FODFs are given in Figure 6(b). The transition from the planar isotropic state in Figure 6(b) (4) toward the unidirectional state in Figure 6(b) (10) demonstrates the degeneration of the variety of fourth-order fiber orientation tensors towards the unidirectional state, which is defined completely by $\lambda_1 = 1$. Figure 6b (1)–6b (3) corresponds to orientation states represented by orange points in Figure 6(a). These points keep a distance in the d_1 -direction from the boundary of the admissible body, as orientation states at the boundary itself, correspond to Dirac distributions into two directions each (see, [13, Figure 9]). In analogy, Figure 6(b)(7) to (b)(9) corresponds to points highlighted in magenta in Figure 6(a) and are also located off the boundary of the admissible region. Figure 9 in Bauer and Böhlke [13] contains FODF approximations based on a limited number of discrete fibers aligned along the axes of the orientation coordinate system which correspond to points on the boundary of the admissible region specified by the line $d_1 = -4/35$ and $d_s = 0$ in Figure 6(a). Planar fiber orientation tensors at the boundary of the admissible region directly correspond to orientation states of a limited number of Dirac distributions. This observation explains why experimentally identified fiber orientation tensors obtained from comparably large fiber arrangements may not fill the complete admissible region but fill only a (equally shaped) subregion within the admissible region. In a comparably large fiber arrangement, Dirac distributions are unlikely. The entropy reconstruction scheme contains a basis function involving a direction depended exponential function. Although the slope of an exponential function is rather steep, extreme values of the Lagrange multipliers are necessary to approximate Dirac distributions. Therefore, the entropy reconstruction scheme, which includes numerical integration and a numerical solver, is not completely stable when operating on orientation states at the boundary of the admissible region. As the unidirectional case in Figure 6(b) (10) lies on the radial boundary of the admissible orientation states, the corresponding entropy-based reconstruction FODF degenerates to a single Dirac distribution. The approximation $\hat{\psi}^{\text{me}}$ in this figure is localized, i.e., vanishes for all angles except those pointing along axes of the orientation coordinate system.

The slices defined in Figure 4 and the corresponding FODF approximations in Figures 6(c) and 7(a) and (b) visualize the variety of reconstructed FODF among fourth-order fiber orientation tensors which contract to identical second-order fiber orientation tensors. Any FODF in Figure 6(c) leads to the

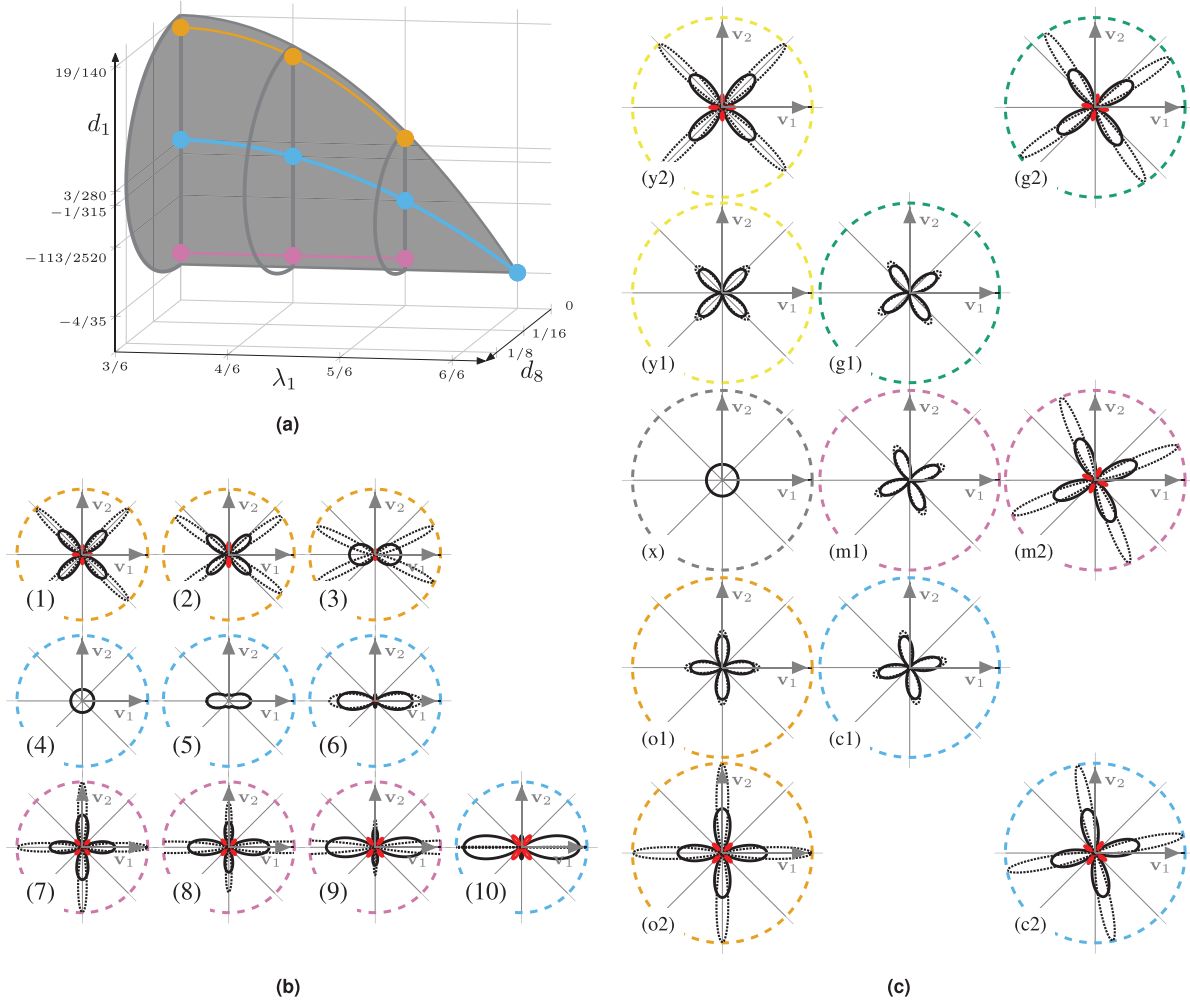


Figure 6. Parameters of points in $\mathcal{N}^{\text{planar}}$, i.e., \mathbb{N} , are listed in Table 2 in Appendix 2. (a) Ten points in the plane of planar orthotropic fiber orientation tensors of fourth-order being a slice of $\mathcal{N}^{\text{planar}}$. The points are used in Figure 6(b). (b) Reconstructed FODF at specific points which are defined in Figure 6(a). A legend is given in Figure 5. (c) Reconstructed FODF at specific points along paths defined in Figure 4(a). The radial spacing of the plots along the green and blue paths are not to true scale to allow for larger plots (a) legend is given in Figure 5.

planar isotropic second-order fiber orientation tensor $\mathbf{N}(\lambda_1 = 1/2)$. In analogy, any FODF in Figure 7(a) has an identical second-order fiber orientation tensor being $\mathbf{N}(\lambda_1 = 2/3)$. From this viewpoint, each of the Figures 6(c) and 7(a) or 7(b) visualizes the variety of planar fourth-order fiber orientation tensors for a fixed second-order orientation tensor. Figure 6(c) shows the redundancy inside $\mathcal{N}^{\text{planar}}$ identified in equation (27) as FODFs with identical radial distance to the centered Figure 6(c) (x) only differ by a rotation. In contrast, interference of the non-vanishing second-order contribution with the fourth-order contribution in Figure 7(a) and (b) leads to a variety of FODF approximations. The developed views on $\mathcal{N}^{\text{planar}}$ based on slices and selected points can be reused to analyze and visualize any quantity which depends on planar fourth-order fiber orientation tensors.

2.3.5. Reconstruction solely based on second-order fiber orientation tensors. If fourth-order fiber orientation information is not available, the parameter space of reconstructed FODFs degenerates to one parameter, e.g., $1/2 \leq \lambda_1 \leq 1$, which defines the second-order fiber orientation tensor. Missing fourth-order fiber orientation information implies vanishing fourth-order deviators, and therefore leads to FODF

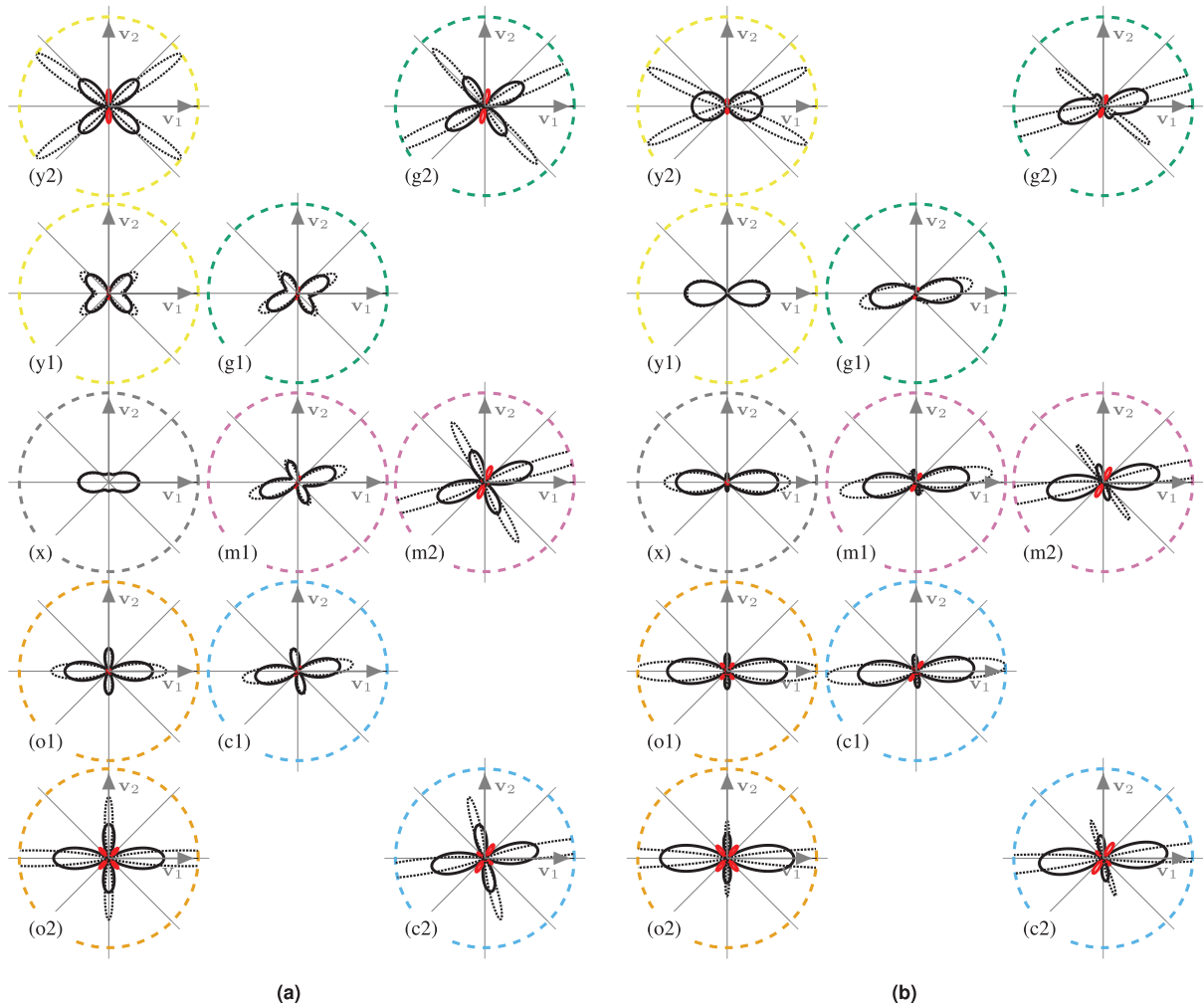


Figure 7. Reconstructed FODF along several paths. The radial spacing of the plots along the green and blue paths are not to true scale to allow for larger plots. A legend is given in Figure 5 and parameters of the points in $\mathcal{N}^{\text{planar}}$, i.e., $\mathbb{N}^{\text{planar}}$, are listed in Table 2 in Appendix 2. (a) Paths are defined in Figure 4b. (b) Paths are defined in Figure 4(c).

reconstructions with $\hat{\psi}(\varphi, \lambda_1, p_1 = 0, p_2 = 0)$ in equation (52) and $\hat{\psi}^{\text{mc}}(\varphi, L, f_1, f_2, g_1 = 0, g_2 = 0)$ in equation (71). Figure 8 shows the influence of λ_1 on reconstructed FODFs for the methods used in the previous section and in addition for the FODF approximation obtained by the exact closure approximation [15]. The exact closure approximation is frequently used, e.g., in [9–11,37] and postulates a one-to-one correspondence between a given second-order fiber orientation tensor and an a priori unknown FODF $\hat{\psi}^{\text{exact closure}}$ of special shape. In the general 3D case, this FODF can be identified by solving elliptic integrals [15]. For the planar case, [11] gives explicit formulas which, combined with equation (14), lead to

$$\hat{\psi}^{\text{exact closure}}(\varphi, \lambda_1) = \frac{1}{2\pi\lambda_1^2 + (1 - 2\lambda_1)\cos(\varphi)^2} \frac{(1 - \lambda_1)\lambda_1}{\cos(\varphi)^2}. \quad (77)$$

Visualization of equation (77) for five values of λ_1 is given in Figure 8. If missing fourth-order orientation information is compensated by deploying closure approximations, the variety of resulting FODFs shown in Figures 6(b) and 7 is not reachable. Instead, the parameter space of structurally differing resulting FODFs degenerates to the parameter space of the second-order orientation tensor within the orientation coordinate system. If closure approximations are used in the context of planar fiber orientations, the complete orientation information is contained within two scalar parameters. One scalar

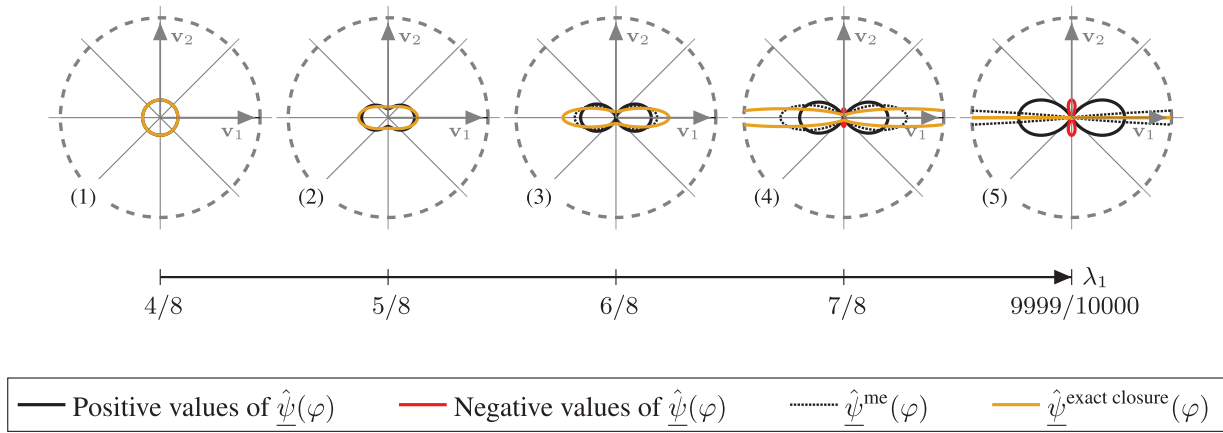


Figure 8. Influence of λ_1 on reconstructed FODF for selected reconstruction methods based on second-order fiber orientation tensors. For $\lambda_1 = 1/2$, all approximations coincide.

parameter specifies the orientation coordinate system and the other parameter specifies the structure of the second-order fiber orientation tensor. In contrast, if the discrete orientation of each single fiber is known, e.g., based on direct fiber simulation [38], the variety of resulting FODF is generic. However, averaged information of such a discrete set of fibers expressed by fiber orientation tensors is still limited.

3. Summary and conclusion

Planar fourth-order fiber orientation tensors describe the fiber orientation in many sheet-like fiber-reinforced composites. The variety of these tensors is known [13]. The variety of reconstructed FODFs based on planar fourth-order fiber orientation tensors is studied in this work leading to the following insights:

1. Based on the set of admissible planar fiber orientation tensors in Bauer and Böhlke [13], a minimal set of admissible and distinct planar fiber orientation tensors of fourth order $\mathcal{N}^{\text{planar}}$ is derived and given in equation (28). This set is the basis for studies on the influence of planar fourth-order fiber orientation tensors on any physical quantity or material function which is formulated in this directional measure.
2. The variety of reconstructed FODF is visualized by an arrangement of polar plots which mimics the shape of the admissible and distinct parameter space. This arrangement or view is generic and may be applied to study the dependence of other quantities on planar fourth-order fiber orientation tensors.
3. Reconstructed FODF based on truncated series expansion within a 3D framework is identified to be not planar as the central state in three dimensions is isotropic.
4. A 2D formulation of planar fiber orientation tensors is introduced and linked to parameterizations of planar fiber orientation tensors in three dimensions. The central, i.e., “isotropic,” state in two dimensions is planar isotropic.
5. Within the 2D framework, it is shown that interference of second- and fourth-order contributions leads to the variety of reconstructed FODF based on truncated Fourier series.
6. Visualizations of truncated FODF reconstructions in Figures 6(b) and 7 highlight their limitations and motivate more advanced reconstruction methods. The maximum entropy reconstruction of Müller and Böhlke [14] is explicitly formulated for the general 3D case and recast for the planar case in a 2D framework which leads to a low-dimensional optimization problem. Resulting FODF approximations are normalized and non-negative.
7. For given reconstruction methods, the structural variety of reconstructed FODF based on planar fourth-order fiber orientation tensors is limited. Throughout this work, separation of rigid-body rotations, and thus orientation in space, from structural properties of represented FODFs is accomplished by representations in the orientation coordinate system.

8. Visualization of reconstructed FODFs solely based on second-order fiber orientation tensors, including a reconstruction method based on the exact closure [11,15], closes this paper and motivates higher-order directional measures.

Acknowledgements

J.K.B. acknowledges Nils Meyer for valuable and intensive technical discussions. J.K.B. acknowledges Jonas Hund for valuable support and discussions on visualizations.

Author contributions

J.K.B. contributed to the conceptualization, methodology software, validation, formal analysis, investigation, resources, writing—original draft preparation, writing—review and editing, and visualization. T.B. contributed to the methodology, formal analysis, resources, writing—review and editing, supervision, project administration, and funding acquisition. All authors have read and agreed to the published version of the manuscript.

Declaration of conflicting interests

The author(s) declared no potential conflicts of interest with respect to the research, authorship, and/or publication of this article. The funders had no role in the design of the study; in the collection, analyses, or interpretation of data; in the writing of the manuscript, or in the decision to publish the results.

Funding

The author(s) disclosed receipt of the following financial support for the research, authorship, and/or publication of this article: The research documented in this manuscript has been funded by the Deutsche Forschungsgemeinschaft (DFG, German Research Foundation), project number 255730231, within the International Research Training Group “Integrated engineering of continuous-discontinuous long fiber-reinforced polymer structures” (GRK 2078/2). The support by the German Research Foundation (DFG) is gratefully acknowledged.

ORCID iD

Julian Karl Bauer  <https://orcid.org/0000-0002-4931-5869>

Thomas Böhlke  <https://orcid.org/0000-0001-6884-0530>

Code

Selected parts of the source code of this work are openly available at https://github.com/JulianKarlBauer/planar_fiber_orientation_distributions.

References

- [1] Kanatani, KI. Distribution of directional data and fabric tensors. *Int J Eng Sci* 1984; 22(2): 149–164.
- [2] Advani, SG, and Tucker, III CL. The use of tensors to describe and predict fiber orientation in short fiber composites. *J Rheol* 1987; 31(8): 751–784.
- [3] Böhlke, T, Henning, F, Hrymak, A, et al. *Continuous–discontinuous fiber-reinforced polymers: an integrated engineering approach*. Munich: Carl Hanser Verlag GmbH Co KG, 2019.
- [4] Görthofer, J, Meyer, N, Pallicity, TD, et al. Virtual process chain of sheet molding compound: development, validation and perspectives. *Comp Part B: Eng* 2019; 169: 133–147.
- [5] Pinter, P, Dietrich, S, Bertram, B, et al. Comparison and error estimation of 3D fibre orientation analysis of computed tomography image data for fibre reinforced composites. *NDT & E Int* 2018; 95: 26–35.
- [6] Schöttl, L, Dörr, D, Pinter, P, et al. A novel approach for segmenting and mapping of local fiber orientation of continuous fiber-reinforced composite laminates based on volumetric images. *NDT & E Int* 2020; 110: 102194.
- [7] Kehrer, L, Wood, JT, and Böhlke, T. Mean-field homogenization of thermoelastic material properties of a long fiber-reinforced thermoset and experimental investigation. *J Comp Mater* 2020; 54: 3777–3799.
- [8] Brylka, B. *Charakterisierung und Modellierung der Steifigkeit von langfaserverstärktem Polypropylen*, vol. 10. Karlsruhe: KIT Scientific Publishing, 2017.
- [9] Hessman, PA, Welschinger, F, Hornberger, K, et al. On mean field homogenization schemes for short fiber reinforced composites: unified formulation, application and benchmark. *Int J Solids Struct* 2021; 230–231: 111141.
- [10] Goldberg, N, Ospald, F, and Schneider, M. A fiber orientation-adapted integration scheme for computing the hyperelastic tucker average for short fiber reinforced composites. *Comput Mech* 2017; 60(4): 595–611.

- [11] Görthofer, J, Schneider, M, Ospald, F, et al. Computational homogenization of sheet molding compound composites based on high fidelity representative volume elements. *Comput Mater Sci* 2020; 174: 109456.
- [12] Schemmann, M, Görthofer, J, Seelig, T, et al. Anisotropic meanfield modeling of debonding and matrix damage in SMC composites. *Comp Sci Technol* 2018; 161: 143–158.
- [13] Bauer, JK, and Böhlke, T. Variety of fiber orientation tensors. *Math Mech Solids*. Epub ahead of print 16 December 2021. DOI:10.1177/10812865211057602.
- [14] Müller, V, and Böhlke, T. Prediction of effective elastic properties of fiber reinforced composites using fiber orientation tensors. *Comp Sci Technol* 2016; 130: 36–45.
- [15] Montgomery-Smith, S, He, W, Jack, DA, et al. Exact tensor closures for the three-dimensional Jeffery’s equation. *J Fluid Mech* 2011; 680: 321–335.
- [16] Harris, CR, Millman, KJ, van der Walt, SJ, et al. Array programming with NumPy. *Nature* 2020; 585(7825): 357–362.
- [17] Meurer, A, Smith, CP, Paprocki, M, et al. Sympy: symbolic computing in Python. *PeerJ Comp Sci* 2017; 3: e103.
- [18] Cintra, JS, Jr, and Tucker, III CL. Orthotropic closure approximations for flow-induced fiber orientation. *J Rheol* 1995; 39(6): 1095–1122.
- [19] Chung, DH, and Kwon, TH. Invariant-based optimal fitting closure approximation for the numerical prediction of flow-induced fiber orientation. *J Rheol* 2002; 46(1): 169–194.
- [20] Köbler, J, Schneider, M, Ospald, F, et al. Fiber orientation interpolation for the multiscale analysis of short fiber reinforced composite parts. *Comput Mech* 2018; 61(6): 729–750.
- [21] Spencer, A. A note on the decomposition of tensors into traceless symmetric tensors. *Int J Eng Sci* 1970; 8(6): 475–481.
- [22] Schöttl, L, Weidenmann, KA, Sabiston, T, et al. Fiber bundle tracking method to analyze sheet molding compound microstructure based on computed tomography images. *NDT & E Int* 2021; 117: 102370.
- [23] Thomson, W. Elements of a mathematical theory of elasticity. *Philos T Royal Soc London* 1856(146): 481–498.
- [24] Mandel, J. Généralisation de la théorie de plasticité de WT Koiter. *Int J Solids Struct* 1965; 1(3): 273–295.
- [25] Mehrabadi, MM, and Cowin, SC. Eigentensors of linear anisotropic elastic materials. *Quart J Mech Appl Math* 1990; 43(1): 15–41.
- [26] Cowin, SC, and Mehrabadi, MM. Anisotropic symmetries of linear elasticity. *Appl Mech Rev* 1995; 48(5): 247–285.
- [27] Blinowski, A, Ostrowska-Maciejewska, J, and Rychlewski, J. Two-dimensional Hooke’s tensors-isotropic decomposition, effective symmetry criteria. *Arch Mech* 1996; 48(2): 325–345.
- [28] Vianello, M. An integrity basis for plane elasticity tensors. *Arch Mech* 1997; 49(1): 197–208.
- [29] Desmorat, B, and Desmorat, R. Tensorial polar decomposition of 2d fourth-order tensors. *Comp Rend Méc* 2015; 343(9): 471–475.
- [30] Vannucci, P. *Anisotropic elasticity*. Singapore: Springer, 2018.
- [31] ABmus, M, Eisenträger, J, and Altenbach, H. Projector representation of isotropic linear elastic material laws for directed surfaces. *ZAMM: J Appl Math Mech* 2017; 97(12): 1625–1634.
- [32] Forte, S, and Vianello, M. A unified approach to invariants of plane elasticity tensors. *Meccanica* 2014; 49(9): 2001–2012.
- [33] Jack, DA, and Smith, DE. Assessing the use of tensor closure methods with orientation distribution reconstruction functions. *J Comp Mater* 2004; 38(21): 1851–1871.
- [34] Rychlewski, J. A qualitative approach to Hookes tensors. part I. *Arch Mech* 2000; 52(4–5): 737–759.
- [35] nschloe. nschloe/fiberoripy: v0.16.10, 2021, <https://github.com/nschloe/quadpy>
- [36] Krylov, VI, and Stroud, AH. *Approximate calculation of integrals*. Chelmsford, MA: Courier Corporation, 2006.
- [37] Schneider, M. The sequential addition and migration method to generate representative volume elements for the homogenization of short fiber reinforced plastics. *Comput Mech* 2017; 59(2): 247–263.
- [38] Meyer, N, Schöttl, L, Bretz, L, et al. Direct bundle simulation approach for the compression molding process of sheet molding compound. *Comp Part A: Appl Sci Manuf* 2020; 132: 105809.
- [39] Cowin, S, and Mehrabadi, M. The structure of the linear anisotropic elastic symmetries. *J Mech Phys Solids* 1992; 40(7): 1459–1471.
- [40] Böhlke, T. *Crystallographic texture evolution and elastic anisotropy: simulation, modeling, and applications*. Shaker Heights, OH: Shaker, 2001.

Appendix I

Kelvin–Mandel notation and completely symmetric tensors of fourth order

This appendix directly follows [13] for the current work to be self-contained. Kelvin–Mandel notation, explicitly introduced in Mandel [24], originating from Thomson [23], discussed in [25,39,40] and also known as normalized Voigt notation, enables compact two-dimensional representations of fourth-order tensors with at least minor symmetry. A fourth-order tensor $\mathbb{A} = A_{ijkl} \mathbf{e}_i \otimes \mathbf{e}_j \otimes \mathbf{e}_k \otimes \mathbf{e}_l$ is minor symmetric if it has both minor symmetries, i.e., $A_{ijkl} = A_{jikl} = A_{ijlk}$ holds. Introducing base tensors in an arbitrary Cartesian basis $\{\mathbf{e}_i\}$ by

$$\begin{aligned}
\mathbf{B}_1 &= \mathbf{e}_1 \otimes \mathbf{e}_1, & \mathbf{B}_4 &= \frac{\sqrt{2}}{2} [\mathbf{e}_2 \otimes \mathbf{e}_3 + \mathbf{e}_3 \otimes \mathbf{e}_2], \\
\mathbf{B}_2 &= \mathbf{e}_2 \otimes \mathbf{e}_2, & \mathbf{B}_5 &= \frac{\sqrt{2}}{2} [\mathbf{e}_1 \otimes \mathbf{e}_3 + \mathbf{e}_3 \otimes \mathbf{e}_1], \\
\mathbf{B}_3 &= \mathbf{e}_3 \otimes \mathbf{e}_3, & \mathbf{B}_6 &= \frac{\sqrt{2}}{2} [\mathbf{e}_2 \otimes \mathbf{e}_1 + \mathbf{e}_1 \otimes \mathbf{e}_2]
\end{aligned} \tag{78}$$

any minor symmetric tensor \mathbb{A} is represented by a six by six matrix of coefficients $A_{\xi\zeta}$

$$\mathbb{A} = A_{ijkl} \mathbf{e}_i \otimes \mathbf{e}_j \otimes \mathbf{e}_k \otimes \mathbf{e}_l = A_{\xi\zeta} \mathbf{B}_\xi \otimes \mathbf{B}_\zeta, \tag{79}$$

with ξ and ζ summing from 1 to 6. Complete index symmetry of a tensor \mathbb{N} implies the structure

$$\mathbb{N} = \left[\begin{array}{ccc|ccc} N_{11}^{(4)} & N_{12}^{(4)} & N_{13}^{(4)} & \sqrt{2}N_{14}^{(4)} & \sqrt{2}N_{15}^{(4)} & \sqrt{2}N_{16}^{(4)} \\ & N_{22}^{(4)} & N_{23}^{(4)} & \sqrt{2}N_{24}^{(4)} & \sqrt{2}N_{25}^{(4)} & \sqrt{2}N_{26}^{(4)} \\ & & N_{33}^{(4)} & \sqrt{2}N_{34}^{(4)} & \sqrt{2}N_{35}^{(4)} & \sqrt{2}N_{36}^{(4)} \\ \hline & \text{major symmetric} & & 2N_{23}^{(4)} & 2N_{36}^{(4)} & 2N_{25}^{(4)} \\ & & & & 2N_{13}^{(4)} & 2N_{14}^{(4)} \\ & & & & & 2N_{12}^{(4)} \end{array} \right] \mathbf{B}_\xi \otimes \mathbf{B}_\zeta. \tag{80}$$

As complete index symmetry implies major index symmetry, the coefficient matrix in equation (80) is symmetric. In equation (80), indices of redundant tensor coefficients are colored. The redundancy implies that six coefficients in the upper left quadrant and nine coefficients in the upper right quadrant of the coefficients in Kelvin–Mandel representation define a completely symmetric tensor. This motivates a short hand notation “completely symmetric” (see, e.g., equation (15)).

Appendix 2

Parameter sets in polar plots

Table 2. Parameter combinations leading to selected fourth-order fiber orientation tensors, which are used to generate polar plots in Figures 6(b) and (c) and 7(a) and (b). Numerical values of the Lagrange multipliers in equation (71) are given with limited precision and absolute values smaller than $10^{-5} = 1\text{E}^{-5}$ set to zero.

Figures	λ_1	$\hat{\beta}$	\hat{r}	d_1	d_8	L	f_1	f_2	g_1	g_2
6b (1)	1/2	$\pi/2$	9/80	69/560	0	4.42E ⁰	0	0	-5.30E ⁰	0
6b (2)	2/3	$\pi/2$	1/10	61/630	0	6.43E ⁰	-7.69E ⁰	0	-6.12E ⁰	0
6b (3)	5/6	$\pi/2$	1/16	89/5040	0	1.66E ¹	-2.46E ¹	0	-9.77E ⁰	0
6b (4)	1/2	0	0	3/280	0	8.38E ⁻¹	0	0	0	0
6b (5)	2/3	0	0	-1/315	0	9.56E ⁻¹	-6.67E ⁻¹	0	1.20E ⁻¹	0
6b (6)	5/6	0	0	-113/2520	0	1.45E ⁰	-1.34E ⁰	0	6.49E ⁻¹	0
6b (7)	1/2	$-\pi/2$	9/80	-57/560	0	4.42E ⁰	0	0	5.30E ⁰	0
6b (8)	2/3	$-\pi/2$	1/10	-13/126	0	5.01E ⁰	-3.63E ⁻¹	0	5.89E ⁰	0
6b (9)	5/6	$-\pi/2$	1/16	-541/5040	0	8.26E ⁰	-8.34E ⁻¹	0	9.13E ⁰	0
6b (10)	1	0	0	-4/35	0	1.81E ³	-5.51E ⁰	1.03E ¹	1.81E ³	-5.18E ⁰
6c (x)	1/2	0	0	3/280	0	8.38E ⁻¹	0	0	0	0
6c (o1)	1/2	$-\pi/2$	1/16	-29/560	0	1.15E ⁰	0	0	1.16E ⁰	0
6c (o2)	1/2	$-\pi/2$	9/80	-57/560	0	4.42E ⁰	0	0	5.30E ⁰	0
6c (c1)	1/2	$-\pi/4$	1/16	3/280 - $\sqrt{2}/32$	$\sqrt{2}/32$	1.15E ⁰	0	0	8.20E ⁻¹	-8.20E ⁻¹
6c (c2)	1/2	$-\pi/4$	9/80	3/280 - $9\sqrt{2}/160$	$9\sqrt{2}/160$	4.42E ⁰	0	0	3.75E ⁰	-3.75E ⁰
6c (m1)	1/2	0	1/16	3/280	1/16	1.15E ⁰	0	0	0	-1.16E ⁰
6c (m2)	1/2	0	9/80	3/280	9/80	4.42E ⁰	0	0	0	-5.30E ⁰

(continued)

Table 2. Continued

Figures	λ_1	$\hat{\beta}$	\hat{r}	d_1	d_8	L	f_1	f_2	g_1	g_2
6c (g1)	1/2	$\pi/4$	1/16	$3/280 + \sqrt{2}/32$	$\sqrt{2}/32$	1.15E ⁰	0	0	-8.20E ⁻¹	-8.20E ⁻¹
6c (g2)	1/2	$\pi/4$	9/80	$3/280 + 9\sqrt{2}/160$	$9\sqrt{2}/160$	4.42E ⁰	0	0	-3.75E ⁰	-3.75E ⁰
6c (y1)	1/2	$\pi/2$	1/16	41/560	0	1.15E ⁰	0	0	-1.16E ⁰	0
6c (y2)	1/2	$\pi/2$	9/80	69/560	0	4.42E ⁰	0	0	-5.30E ⁰	0
7a (x)	2/3	0	0	-1/315	0	9.56E ⁻¹	-6.67E ⁻¹	0	1.20E ⁻¹	0
7a (o1)	2/3	$-\pi/2$	1/18	-37/630	0	1.30E ⁰	-4.54E ⁻¹	0	1.30E ⁰	0
7a (o2)	2/3	$-\pi/2$	1/10	-13/126	0	5.01E ⁰	-3.63E ⁻¹	0	5.89E ⁰	0
7a (c1)	2/3	$-\pi/4$	1/18	$-\sqrt{2}/36 - 1/315$	$\sqrt{2}/36$	1.31E ⁰	-5.86E ⁻¹	3.36E ⁻¹	9.53E ⁻¹	-8.36E ⁻¹
7a (c2)	2/3	$-\pi/4$	1/10	$-\sqrt{2}/20 - 1/315$	$\sqrt{2}/20$	5.20E ⁰	-1.39E ⁰	2.51E ⁰	4.22E ⁰	-4.15E ⁰
7a (m1)	2/3	0	1/18	-1/315	1/18	1.32E ⁰	-9.01E ⁻¹	4.71E ⁻¹	1.20E ⁻¹	-1.19E ⁰
7a (m2)	2/3	0	1/10	-1/315	1/10	5.69E ⁰	-3.93E ⁰	3.60E ⁰	8.21E ⁻²	-5.99E ⁰
7a (g1)	2/3	$\pi/4$	1/18	$-1/315 + \sqrt{2}/36$	$\sqrt{2}/36$	1.33E ⁰	-1.21E ⁰	3.30E ⁻¹	-7.18E ⁻¹	-8.40E ⁻¹
7a (g2)	2/3	$\pi/4$	1/10	$-1/315 + \sqrt{2}/20$	$\sqrt{2}/20$	6.21E ⁰	-6.56E ⁰	2.59E ⁰	-4.26E ⁰	-4.35E ⁰
7a (y1)	2/3	$\pi/2$	1/18	11/210	0	1.33E ⁰	-1.33E ⁰	0	-1.07E ⁰	0
7a (y2)	2/3	$\pi/2$	1/10	61/630	0	6.43E ⁰	-7.69E ⁰	0	-6.12E ⁰	0
7b (x)	5/6	0	0	-113/2520	0	1.45E ⁰	-1.34E ⁰	0	6.49E ⁻¹	0
7b (o1)	5/6	$-\pi/2$	5/144	-401/5040	0	2.00E ⁰	-9.88E ⁻¹	0	1.96E ⁰	0
7b (o2)	5/6	$-\pi/2$	1/16	-541/5040	0	8.26E ⁰	-8.34E ⁻¹	0	9.13E ⁰	0
7b (c1)	5/6	$-\pi/4$	5/144	$-113/2520 - 5\sqrt{2}/288$	$5\sqrt{2}/288$	2.04E ⁰	-1.29E ⁰	9.33E ⁻¹	1.59E ⁰	-9.71E ⁻¹
7b (c2)	5/6	$-\pi/4$	1/16	$-113/2520 - \sqrt{2}/32$	$\sqrt{2}/32$	9.37E ⁰	-4.00E ⁰	7.92E ⁰	6.69E ⁰	-6.27E ⁰
7b (m1)	5/6	0	5/144	-113/2520	5/144	2.07E ⁰	-1.93E ⁰	1.25E ⁰	6.77E ⁻¹	-1.36E ⁰
7b (m2)	5/6	0	1/16	-113/2520	1/16	1.23E ¹	-1.20E ¹	1.17E ¹	5.68E ⁻¹	-9.41E ⁰
7b (g1)	5/6	$\pi/4$	5/144	$-113/2520 + 5\sqrt{2}/288$	$5\sqrt{2}/288$	1.95E ⁰	-2.37E ⁰	7.97E ⁻¹	-1.91E ⁻¹	-9.20E ⁻¹
7b (g2)	5/6	$\pi/4$	1/16	$-113/2520 + \sqrt{2}/32$	$\sqrt{2}/32$	1.55E ¹	-2.09E ¹	8.87E ⁰	-6.48E ⁰	-7.31E ⁰
7b (y1)	5/6	$\pi/2$	5/144	-17/1680	0	1.86E ⁰	-2.47E ⁰	0	-5.16E ⁻¹	0
7b (y2)	5/6	$\pi/2$	1/16	89/5040	0	1.66E ¹	-2.46E ¹	0	-9.77E ⁰	0